UNIVERSITÀ DEGLI STUDI DI PADOVA

DIPARTIMENTO DI INGEGNERIA DELL'INFORMAZIONE

DIPARTIMENTO DI INGEGNERIA DELL'INFORMAZIONE

CORSO DI LAUREA MAGISTRALE IN BIOINGEGNERIA

Upper limb kinematics in functional tasks during standing

Relatore: Dott.ssa Formaggio Emanuela

Laureanda: Guida Sara

Correlatori: Dott.ssa Contessa Paola, Dott.ssa Venturini Erika

ANNO ACCADEMICO 2023-2024

Data di laurea 05/03/2024

ABSTRACT IN ENGLISH

The purpose of this thesis is to create a method for analyzing the features of 3D arm movement, along with consequent thorax and pelvis motions, during functional tasks in both healthy controls, comparing their dominant and non-dominant limbs, and in individuals affected by upper limb lymphedema, comparing the affected limb with the unaffected one.

Lymphedema is a manifestation of insufficient lymphatic system function, following, in this case, the removal of lymphatic axillary nodes during radical breast surgery. The primary outcome is the swelling of the affected limb, resulting from the accumulation of substances and adipose tissue in the extracellular space. This condition can lead to various complications, including decreased mobility of the shoulder joint.

This study involved ten healthy female controls and two female subjects affected by upper limb lymphedema. Participants were instructed to perform six different motion tasks three consecutive times, including elevation in the sagittal plane with both arms, elevation in the scapular plane with both arms, circumduction, frontal reaching, lateral reaching, and upward reaching done with both one and both arms. Kinematic data were collected using a stereophotogrammetric system with retroreflective markers placed on the upper body during the execution of these functional tasks while standing.

The proposed method starts by segmenting the movement, distinguishing the three different repetitions, using the data of the markers placed on the lateral epicondyle of both elbows (labelled RELB and LELB). Then the instant of maximum amplitude in the movement is determined. Once the intervals of motion are obtained, for each repetition of the functional task, markers RELB and LELB are used to compute the total path length taken by the arms and the mean velocity of execution. To explore compensatory movement of the thorax in the plane xy, the displacement of the segment linking the markers placed on the acromio-clavicular joints (labelled RSHO and LSHO) between the starting position and the reaching maximum amplitude position is computed, in terms of the area enclosed by the two segments. With the same purpose, but in the yz plane, the elbow's trajectory in the circumduction tasks is plotted in both the laboratory and the thorax coordinate systems. The area enclosed in each curve is computed using the trapezoid method to compare the amplitude of the movement trajectory in the two reference frames. Finally, the angular excursion of the thorax over the pelvis and of the pelvis

over the laboratory have been evaluated by computing joint angles with the Grood & Suntay method.

Analysis of the results indicates pronounced asymmetry between limbs in patients with upper limb lymphedema across all computed parameters: in terms of path length and velocity, the values gained are always higher for the unaffected limb, and in terms of thorax compensation movements, these are more present when the functional task is executed with the affected limb. Conversely, in healthy controls, differences between dominant and non-dominant arms are generally not statistically significant, except in select cases. Control subjects typically exhibit slightly higher path length values for the dominant arm and higher velocity values for the non-dominant arm. Trunk compensation movements are more pronounced when tasks are executed with the non-dominant arm. Comparing patients with upper limb lymphedema to control subjects, asymmetry between upper limbs is more pronounced in patients, particularly in one of the two patients, with patients consistently exhibiting lower path length and velocity values compared to controls.

Therefore, as evidenced by the results, the analysis of upper limb kinematics, with particular attention to trunk compensatory movements, could play a significant role in evaluating the effectiveness of therapy and optimizing it.

ABSTRACT IN ITALIANO

Lo scopo di questa tesi è la realizzazione di un metodo per analizzare le caratteristiche del movimento tridimensionale del braccio, insieme ai conseguenti movimenti del torace e del bacino, durante l'esecuzione di task funzionali da parte di soggetti sani di controllo e di soggetti affetti da linfedema agli arti superiori.

Il linfedema è una manifestazione del fallimento del sistema linfatico, in questo contesto dovuto alla rimozione dei nodi linfatici ascellari in seguito a un'operazione di dissezione radicale del seno. Il risultato principale del linfedema all'arto superiore è il rigonfiamento dell'arto interessato, dovuto all'accumulo di sostanze e di tessuto adiposo nello spazio extracellulare. La presenza di linfedema può comportare molteplici conseguenze, tra cui la diminuzione della mobilità dell'articolazione della spalla.

Questo studio ha coinvolto dieci soggetti sani di sesso femminile e due soggetti di sesso femminile affetti da linfedema all'arto superiore. Alle partecipanti è stato chiesto di eseguire stando in piedi sei task funzionali per tre volte consecutive: elevazione bilaterale nel piano sagittale, elevazione bilaterale nel piano scapolare, circonduzione, reaching frontale, reaching in alto e reaching laterale. I dati cinematici durante l'esecuzione di questi task sono stati raccolti utilizzando un sistema stereofotogrammetrico con marcatori retroriflettenti posizionati sulla parte superiore del corpo dei soggetti.

Il metodo proposto inizia segmentando il movimento, ossia distinguendo le tre ripetizioni di ogni task, sfruttando i dati dei marcatori posizionati sull'epicondilo laterale di entrambi i gomiti (denominati RELB e LELB). Successivamente, viene calcolato l'istante di raggiungimento della massima ampiezza. Una volta ottenuti gli intervalli di tempo in cui il soggetto è in movimento, per ogni ripetizione del task funzionale in esame, vengono calcolate la lunghezza totale del percorso svolto e la velocità media con cui questo viene eseguito, usando sempre i marcatori RELB e LELB. Per studiare i movimenti compensatori del tronco nel piano xy, viene calcolato lo spostamento tra l'istante di inizio del movimento e l'istante di raggiungimento della massima ampiezza del segmento che congiunge i marcatori sulle due articolazioni acromio-clavicolari (denominati RSHO e LSHO). Questo spostamento viene valutato come l'area racchiusa tra i due segmenti. Con lo stesso scopo, ma nel piano yz, viene visualizzata la traiettoria dei marcatori sui gomiti durante i task di circonduzione sia rispetto al sistema di

riferimento di laboratorio che rispetto al sistema di riferimento del tronco. L'area racchiusa in ciascuna curva viene quindi calcolata utilizzando il metodo del trapezio per confrontare l'ampiezza della traiettoria di movimento nei due sistemi di riferimento. Infine, l'escursione angolare del torace rispetto al bacino e del bacino rispetto al laboratorio è stata valutata calcolando gli angoli articolari con il metodo di Grood & Suntay.

I risultati mostrano una marcata asimmetria tra gli arti su tutti i parametri calcolati nei soggetti affetti da linfedema: in termini di lunghezza del percorso e velocità, i valori ottenuti sono sempre più alti per l'arto non affetto e, in termini di movimenti compensatori del torace, questi sono più evidenti quando il task funzionale viene eseguito con l'arto affetto. Al contrario, nei soggetti di controllo, le differenze tra braccio dominante e non-dominante non sono generalmente statisticamente significative, tranne in alcuni casi. I soggetti di controllo mostrano tipicamente valori leggermente più alti della lunghezza del percorso per il braccio dominante e valori di velocità più alti per il braccio non-dominante, mentre i movimenti compensatori del tronco sono più evidenti quando i compiti vengono eseguiti con il braccio non-dominante. Confrontando i soggetti con linfedema all'arto superiore e i soggetti di controllo, l'asimmetria tra gli arti superiori è più evidente nei soggetti con linfedema; inoltre, tali soggetti mostrano valori inferiori di lunghezza del percorso e velocità rispetto ai controlli.

Quindi, come si può dedurre dai risultati, l'analisi della cinematica dell'arto superiore, con particolare attenzione ai movimenti compensatori del tronco, potrebbe svolgere un ruolo importante nella valutazione dell'efficacia di una terapia e nell'ottimizzazione di essa.

TABLE OF CONTENTS

INTRODUCTION

The study of upper limb kinematics during functional tasks holds significant relevance in the realm of biomechanics and clinical research. This thesis stems from a research project currently undergoing at the Department of Neuroscience, University of Padova, on patients affected by mono- or bilateral upper limb lymphedema that aims at comparing the effectiveness of traditional treatment with an experimental treatment (traditional treatment combined with water-based exercise treatment and telerehabilitation) [1]. The evaluations encompass clinical parameters (blood tests), assessments of muscle strength, bioimpedance measurements, and changes in mobility assessed through 3D kinematic analysis of the upper limb. The latter point is the focus of this research work.

Lymphedema is a manifestation of lymphatic system failure and unbalanced lymphatic transport. It can be an isolated phenomenon, or it can be associated with a variety of other systemic disorders. Its nature can be acute, transitory, or chronic. It may result from congenital lymphatic dysplasia or dysplasia gained after a radical dissection operation, such as the removal of axillary and retroperitoneal nodules. In both cases, the main disorder is the overall reduction of lymphatic transport resulting in the swelling of the affected body area (Figure 1). The accumulation of water, plasma proteins, extravascular blood cells, and excess stromal products in the extracellular space causes this swelling, which culminates with the proliferation of these elements and the excessive deposition of extracellular matrix substances and adipose tissue. Repeated infections, progressive elephantine trophic changes in the skin, sometimes paralyzing disability, and on rare occasions, the development of highly lethal lymphangiosarcoma are possible consequences of failure to control [2]. It has been demonstrated that the presence of upper limb lymphedema may cause diminished scapular upward rotation, external rotation, and posterior tilt during humeral-thoracic elevation, disrupting the scapulohumeral rhythm. In fact, by comparing the three-dimensional scapular kinematics during arm elevation and depression phases among women with upper limb lymphedema and women without it, it has been shown that there is a decreased joint range of motion in lymphedema patients [3]. This decrease may be

due to factors like increased fat tissues, subcutaneous fluid, and, sometimes, prolonged time since lymphedema diagnosis.

The goal of this thesis is to develop a method that allows the evaluation of upper limb kinematics during the execution of functional tasks by capturing data using a stereophotogrammetric system. The primary objective is to investigate the movements of the upper limbs, with particular attention to compensatory movements of the trunk and pelvis during these activities. The proposed method has been tested on different subjects and from various perspectives. Firstly, it has undergone a comparison between the dominant and non-dominant upper limbs of healthy volunteers to discern any differences in the execution of functional tasks due to arm dominance or preference. Furthermore, the method has been extended to a comparative assessment between control individuals and patients suffering from upper limb lymphedema, thereby exploring potential alterations in the kinematics of the upper limb associated with this pathological condition. To ensure the robustness and reliability of this method, it has been devised by drawing inspiration and by synthesizing insights from the existing literature.

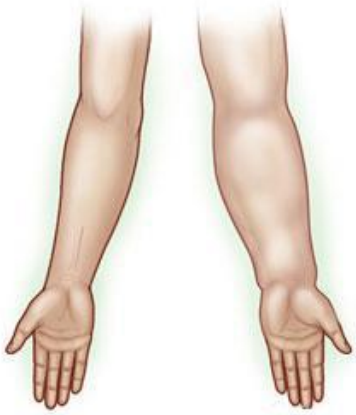

Figure 1. Image of the volar aspect of the upper limbs showing the swelling of the right arm.

1.
MATERIALS

1.1 **Participants**

Within the framework of the study, ten healthy female volunteers aged between 23 and 51 years (31,60 ± 9,95 years) were enrolled as control subjects. Additionally, two female individuals diagnosed with upper limb lymphedema (age 55 and age 53) were included in the study as a patient group (Table 1 and Table 2). The recruitment of these participants was voluntary, and they all granted informed consent. Prior to initiating the experimental phase, on each participant was meticulously conducted a comprehensive set of anatomical measurements: hand thickness, wrist width, elbow width (from lateral to medial epicondyle), distance from the offset of the shoulder and the acromion, leg length (from the anterior iliac spine), knee width, ankle width (from lateral to medial malleolus), and foot length (from heel to the longest toe). These measurements, along with the height of the subject, were indispensable for the seamless integration and optimal functioning of the data acquisition software employed throughout the research. Each control subject also provided information regarding their dominant arm (8 of 10 were right-handed, 2 of 10 were left-handed) (Table 1 and Table 2). This critical detail allowed to explore the comparison between dominant and non-dominant arm in addition to the one between controls and subjects with upper limb lymphedema.

Subject ID	Age	Height [cm]	Weight [kg]	Arm affected by lymphedema
Lymphedema 001	55	160	115	Right
Lymphedema 002	53	64	62	Right

Table 1. Table with the information regarding the subjects affected by upper limb lymphedema included in the patient group.

Subject ID	Age	Height [cm]	Weight [kg]	Dominant arm
Control 002	24	169	60	Right
Control 003	23	165	85	Right
Control 004	24	179	62	Right
Control 006	28	163	50	Right
Control 007	40	168	50	Left
Control 008	23	173	62	Right
Control 009	43	173	60	Right
Control 010	34	160	58	Right
Control 011	26	167	56	Left
Control 012	51	178	70	Right

Table 2. Table with the information regarding the subjects chosen as controls.

1.2 **Functional tasks**

During the experimental phase, each participant was instructed to complete a series of six distinct functional tasks with the upper extremities while standing. Each task was repeated three times at a self-selected speed, with a pause of a few seconds between each repetition. The tasks included: 1) a bilateral frontal arm elevation, where participants were directed to sequentially raise and lower both arms within the sagittal plane; 2) a bilateral scapular arm elevation, requiring participants to raise and lower both arms while maintaining an approximate 45-degree angle; 3) a forward-to-backward arm circumduction, executed with both arms, as well as only

with the right arm and only with the left arm; 4) a frontal reaching task, as to grasp an object positioned in front of the subject; 5) an upward reaching task, as to grasp an object positioned high over the head of the subject; and 6) a lateral reaching task, where the object was placed laterally (Figure 2). Each circumduction and reaching task was also performed three times with both arms, three times with only the right arm, and three times with only the left arm. After each repetition, the subjects were asked to go back to the resting position, which is arm relaxed along the body. It must be noted that the subject Lymphedema001 didn't perform the circumduction and the reaching tasks with both arms simultaneously, rather, these tasks were performed individually, one arm at a time.

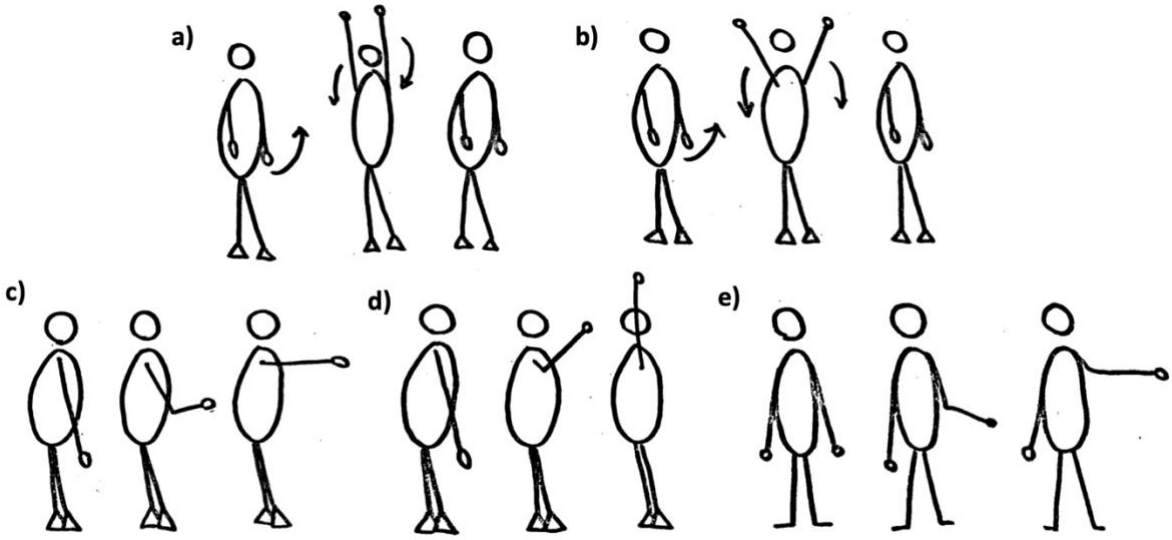

Figure 2. a) Frontal elevation task. b) Scapular elevation task. c) Frontal reaching task executed with one arm. d) Upward reaching task executed with one arm. e) Lateral reaching task executed with one arm.

1.3 **Stereophotogrammetric system**

Stereophotogrammetric motion analysis is extensively used for the assessment of body segment kinematics during gait and other functional tasks. Human movement analysis using stereophotogrammetry involves the reconstruction and estimate of the 3D coordinates of points on an object (the arm segment in our case of functional upper limb tasks), employing measurements made by optoelectronic cameras. This process involves analyzing disparities and triangulation for accurate spatial measurements [4]. In stereophotogrammetric systems for 3D position two or more cameras capture images simultaneously from different angles, enabling the tracking of anatomically relevant points in three dimensions (Figure 3). These points are

typically identified using retroreflective markers, specialized spherical markers designed to reflect light back to its source (Figure 4). These markers typically consist of a substrate covered with a retroreflective material, their retroreflective surface causes incident light to return in the direction it came from, enhancing visibility. In the context of motion capture systems, retroreflective markers are placed on the subject's body at strategic landmarks and serve as passive markers. These markers are employed in conjunction with infrared stroboscopic illumination generated by an array of light-emitting diodes positioned around the lens of each camera that are placed in the space around objects or body parts of interest. When illuminated they efficiently reflect the light back to the camera, allowing the system to track their positions accurately. The stereophotogrammetric system then analyzes pairs of images from different cameras to evaluate disparities between markers. Disparities, indicating the apparent shift in a marker's position between two images, are used to calculate the three-dimensional coordinates of the markers. Triangulation, leveraging camera geometry and disparities, determines the tridimensional positions of retroreflective markers. To ensure the correct attribution of three-dimensional positions to objects in the scene, minimizing errors due to optical distortions or inaccuracies in camera positions, calibration is essential. Calibration in a stereophotogrammetric system involves accurately determining intrinsic parameters (focal length, optical distortion, and perspective axis) and extrinsic parameters (camera position and orientation relative to the scene or objects). This process uses known objects or patterns with defined geometric characteristics (Figure 5). For intrinsic calibration, objects with known patterns are placed at various angles relative to the cameras, while for extrinsic calibration, images of known objects are captured from different perspectives. A specialized software is often employed for automatic calibration, analyzing images of known objects, and automatically calculating intrinsic and extrinsic parameters [5–9].

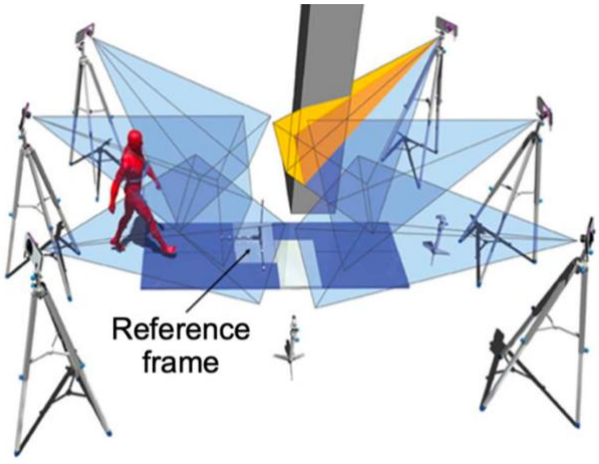

Figure 3. Example of a stereophotogrammetric system setup for the human movement analysis.

Figure 4. Retroreflective (passive) markers.

Figure 5. Calibration wand used in the experimental setup. Its active LEDs are automatically tracked by the motion capture software.

1.4 **Data collection**

During the execution of the functional tasks, data were collected using the Vicon Digital Motion Capture stereophotogrammetric system with a sampling rate of 100 Hz. The system captured data from a set of retroreflective markers placed on the subject on locations of interest to track the position of the pelvis, trunk, and arms in space [10]. All data were referenced to the laboratory coordinate system, with the x-axis representing the medio-lateral direction, the y-axis the antero-posterior direction, and the z-axis the vertical direction (Figure 6).

After data collection, it underwent filtering using a fifth-order spline-interpolating function (Woltring filter in Vicon software [11,12]), and was subsequently stored in either a .csv Excel file or a. mat Matlab file for analysis.

For this thesis, markers were positioned as follows: on the jugular notch where the clavicles meet the sternum (marker named CLAV), on the right/left acromion-clavicular joint (markers named RSHO/LSHO), on the xiphoid process, i.e., most caudal point of the sternum (marker named STRN), over the most caudal point on the right/left lateral epicondyle (markers named RELB/LELB), over the right/left anterior superior iliac spine (markers named RASI/LASI), on the spinous process of the 7th cervical vertebrae (marker named C7), in correspondence of the 10th thoracic vertebrae (marker named T10), over the right/left posterior superior iliac spine (markers named LPSI/RPSI) (Figure 7). Markers CLAV, STRN, T10 and C7 were chosen to create a thorax coordinate system, while the markers RASI, LASI, RPSI and LPSI were selected to realize a pelvis coordinate system. Finally the markers RELB and LELB were considered the most suitable ones for the study of the upper limb kinematics, because they are less sensitive to

occlusion with movement, compared to other positions on the elbow, and because they are not sensitive to arm movements that may be unrelated to shoulder-upper arm movement (like markers on the wrists or fingers which position in space may change due to hand movement). Indeed, when plotting the positional data of each marker over time along the three directions (x, y, and z) to allow a comprehensive view of 3D marker movements throughout the motion tasks, both the markers RELB and LELB displayed features that made them well-suited for displaying the movements of the upper limbs (Figure 8).

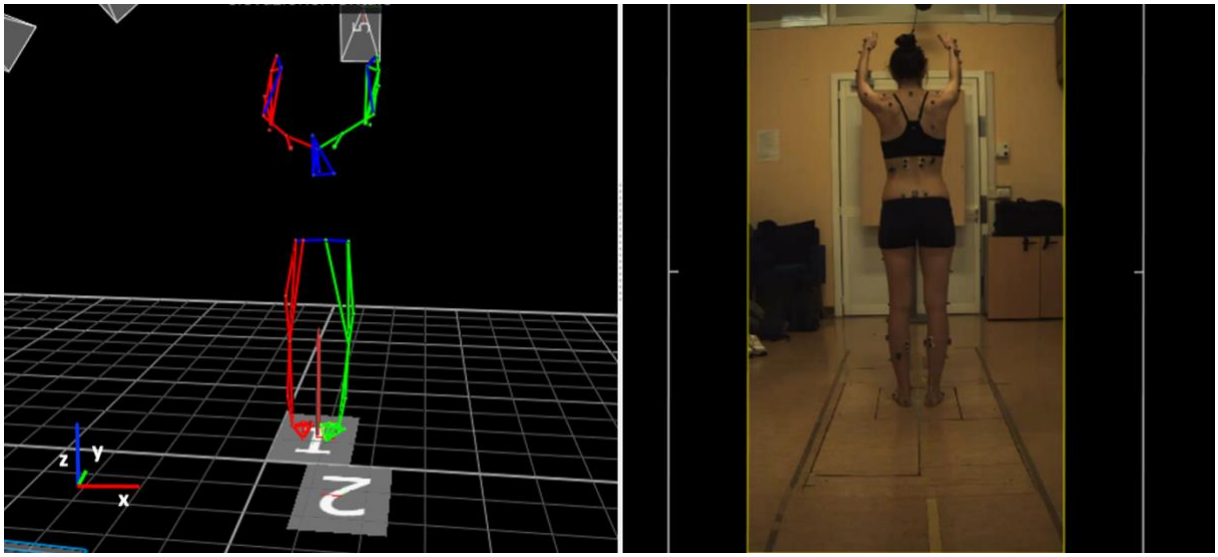

Figure 6. Subject orientation respect to the laboratory coordinate system.

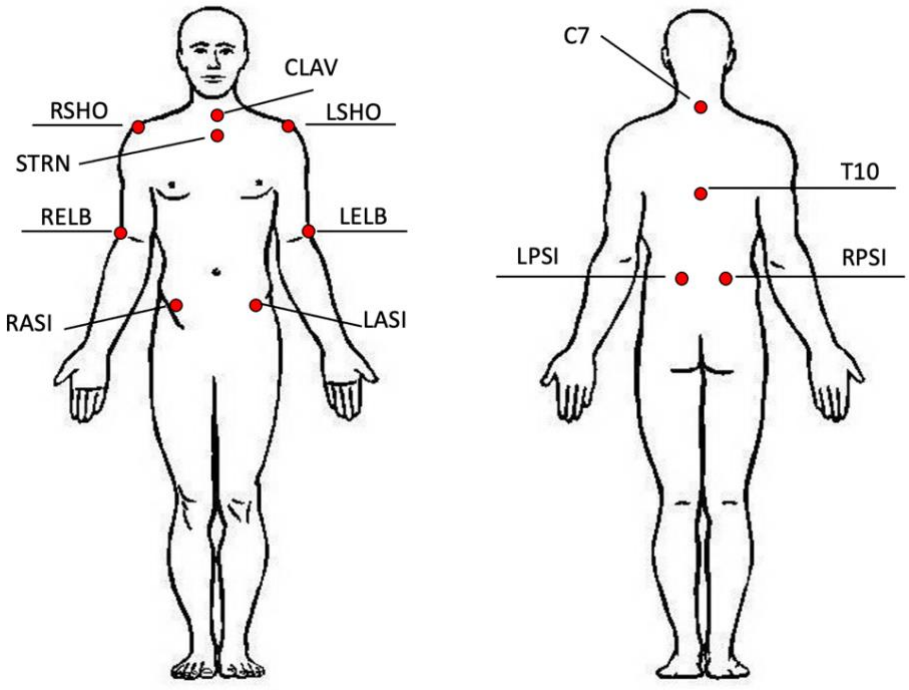

Figure 7. Placement of the markers considered in the study.

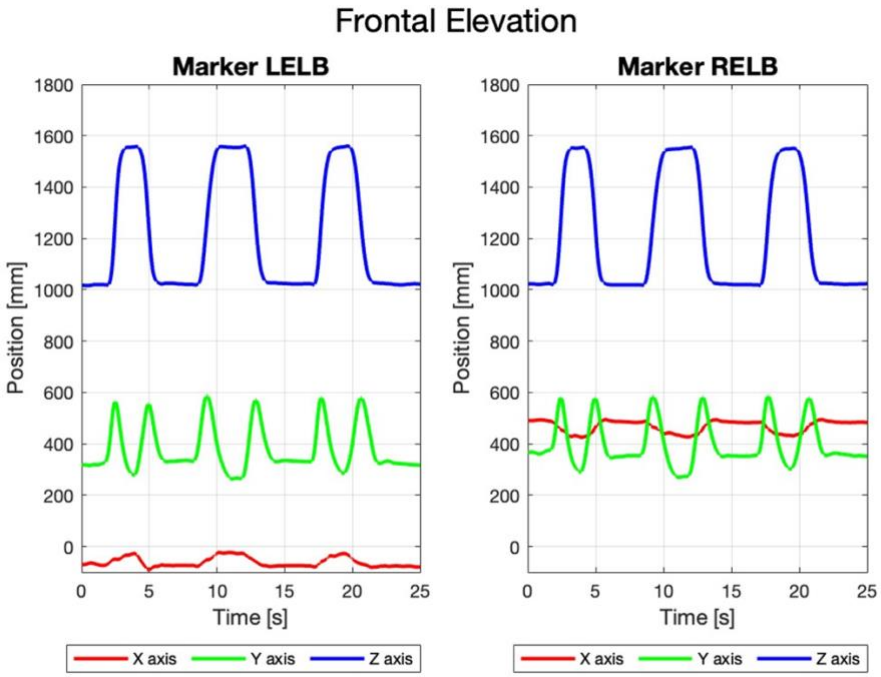

Figure 8. Position over time of the x, y, z axes of the markers LELB and RELB during the frontal elevation task performed with both arms in a representative subject.

2.
METHODS

2.1 **Movement segmentation algorithm**

After loading marker data for a specific task, conducting further analysis requires understanding when the subject is in motion and the number of repetitions of the movement. To achieve this, a movement segmentation algorithm was developed using the Matlab software (MATLAB R2023a). This algorithm provides outputs indicating the start and end instants of each movement repetition. The following is a description of how it operates.

The algorithm begins by calculating the instantaneous velocity of the markers along each direction. This is done by dividing the gradient of the position matrix by the gradient of the time vector. Once the instantaneous velocity is obtained for markers LELB and RELB, the algorithm evaluates resultant vectors for both position and velocity (Equation 1). This involves calculating the vector sum along the three directions: x, y, and z.

$$\text{Resultant Vector } \vec{v} = \sqrt{v_x^2 + v_y^2 + v_z^2}$$

Equation 1. Computation of the generic resultant vector $\vec{v}$, here v_x, v_y, and v_z are the individual components of the vector $\vec{v}$ in the x, y, and z directions, respectively.

When visualizing the resultant positions and velocities (Figure 9), it becomes evident that moments when the subject is stationary correspond to instances where the velocity is almost zero. This observation generally holds true, with exceptions occurring when velocity is nearly null but there's a peak in the position diagram. To pinpoint these instances, the algorithm establishes thresholds for both position and velocity using a 50 ms sliding temporal window. Within each window, it computes the root mean square (RMS) for both position and velocity (Equation 2).

$$\text{RMS}_v = \sqrt{\frac{1}{N}\sum_{i=1}^{N} v_i^2}$$

Equation 2. Root mean square (RMS) of a generic vector $\vec{v}$, here N is the number of samples contained in a window.

Following this, the base 10 logarithm of the RMS is depicted in histograms for both position and velocity, as illustrated in Figure 10. Within these histograms, two discernible regions emerge, each characterized by bins exhibiting higher frequencies. The initial region represents the most frequent values of position or velocity during periods of rest, while the second corresponds to most frequent values during intervals of movement. To determine the threshold values for identifying moments of rest, the algorithm performs a moving average smoothing, with a window length of 10 samples, on the data of the histogram. The smoothing process distinctly highlights the two regions. The algorithm then selects the threshold as the value corresponding to the first point of absolute minimum on the smoothed curve after the first absolute maximum. Performing the inverse logarithm on this chosen value returns the threshold for both position and velocity. Following the establishment of these thresholds, the identification of rest intervals relies on instances where both position and velocity values simultaneously fall below their respective threshold values. Furthermore, the algorithm utilizes the established threshold to quantify the number of movement repetitions (Equation 3). This is accomplished by counting the peaks in the position data that exceed the threshold.

$$\text{countPeaks}(\text{P}, \text{Threshold}) = \sum_{\text{i}=1}^{\text{n}-2} 1\{\text{p}_{\text{i}+1} > \text{p}_{\text{i}} \wedge \text{p}_{\text{i}+1} > \text{p}_{\text{i}+2} \wedge \text{p}_{\text{i}+1} > \text{Threshold}\}$$

$$\text{Number of repetitions} = \text{countPeaks}(\text{P}, \text{Threshold})$$

Equation 3. Count of the number of repetitions performed. $\mathbf{P} = \{\mathbf{p_1}, \mathbf{p_2}, \dots, \mathbf{p_n}\}$ is the series of position data over time, $\mathbf{p_i}$ is the position at the time i, and $\mathbf{1\{condition\}}$ is an indicator function that returns one if the condition is true and zero otherwise.

After obtaining the threshold values, the algorithm seeks the positional index of values lower or equal to these thresholds in the resultant vectors of position and velocity. Subsequently, it performs an intersection between the indices obtained for position and those obtained for velocity, focusing solely on instances where both position and velocity variations are nearly null. This operation yields a vector of indices, where a difference greater than one between consecutive indices signifies an interval of movement. However, considering that the subject may not be entirely still between two repetitions of the movement, the created indices vector may contain gaps that appear to be movement intervals but are not. To address this issue, the algorithm calculates the length of each gap and designates only the longer ones as actual movement intervals, limiting the number of gaps to the count of movement repetitions. After estimating the longest gaps, any remaining gaps are filled within a while loop. Subsequently, all the rest intervals are visualized on the position and velocity diagrams to validate their accuracy (Figure 11).

Upon the detection of the rest intervals, the algorithm records the start and end of each interval in a two-column matrix. This matrix is subsequently employed to calculate movement intervals by determining the gaps between two consecutive rest intervals. Special consideration is given to scenarios where the first repetition starts at the beginning of data acquisition or if the data acquisition concludes with a movement. Consequently, this process generates another matrix characterized by a number of rows equivalent to the count of movement repetitions. The matrix comprises two columns, indicating the instants of the start and end of each repetition. Once the movement intervals have been identified, the algorithm calculates the instant of maximum movement amplitude for each repetition, i.e. the instant when the arm is furthest away from the body along the resultant position and when the resultant velocity is almost null. Specifically, within each movement repetition, the algorithm first searches for the indices of negative peaks in the resultant velocity vector and then determines the index of the maximum position value. Subsequently, the algorithm defines the index of the moment of maximum amplitude as the index of the negative velocity peak closest to the position maximum. The corresponding instances in the time vector are then located, identifying the moments of maximum movement amplitude. After obtaining the movement intervals and the instants of reaching maximum amplitude, or only the former in the case of circumduction, the position and velocity trends over time are plotted. The plots highlight the movement phases and the instances of reaching maximum amplitude (Figure 12).

To comprehensively analyze various tasks, the algorithm is structured around a switch construct that addresses three distinct scenarios: movements executed only with the left arm, movements executed only with the right arm, and movements executed with both arms. In the first two cases, movement segmentation is performed exclusively for one arm, while in the latter case, segmentation is carried out individually for both arms. However, in this latter scenario, the algorithm also calculates instances when both arms are in motion but separately for the two arms assuming they may behave differently (there may be slight differences in the timing of movement between the two arms).

Ultimately, all the time intervals marking the start and end of movements, as well as those indicating the attainment of maximum movement amplitude, are automatically recorded.

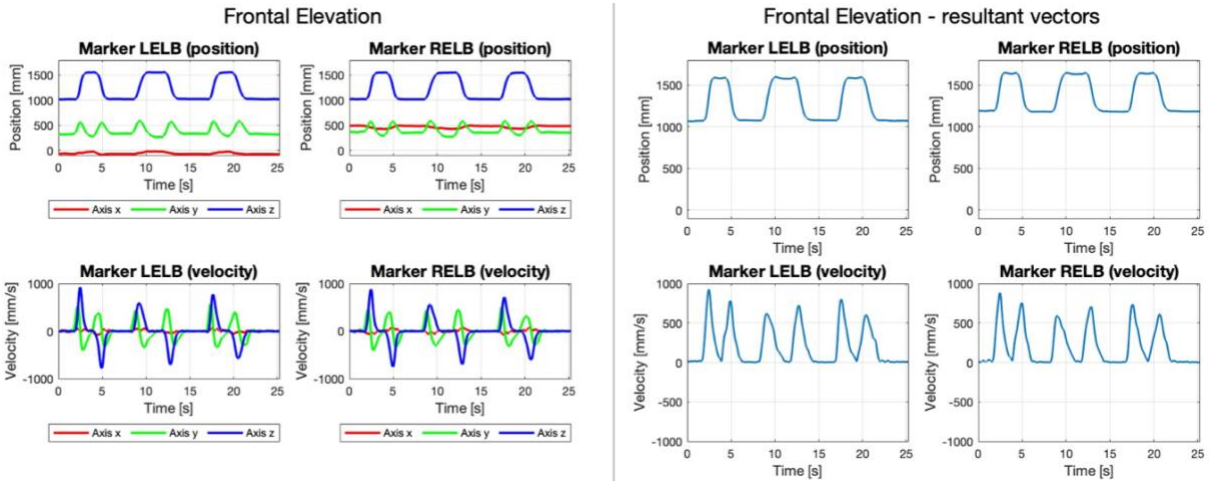

Figure 9. (Left) Position and instantaneous velocity of the markers LELB and RELB over time along the axes x, y and z during the frontal elevation task in one representative subject. (Right) Resultant vectors of position and velocity of the markers LELB and RELB during the frontal elevation task in a representative control subject.

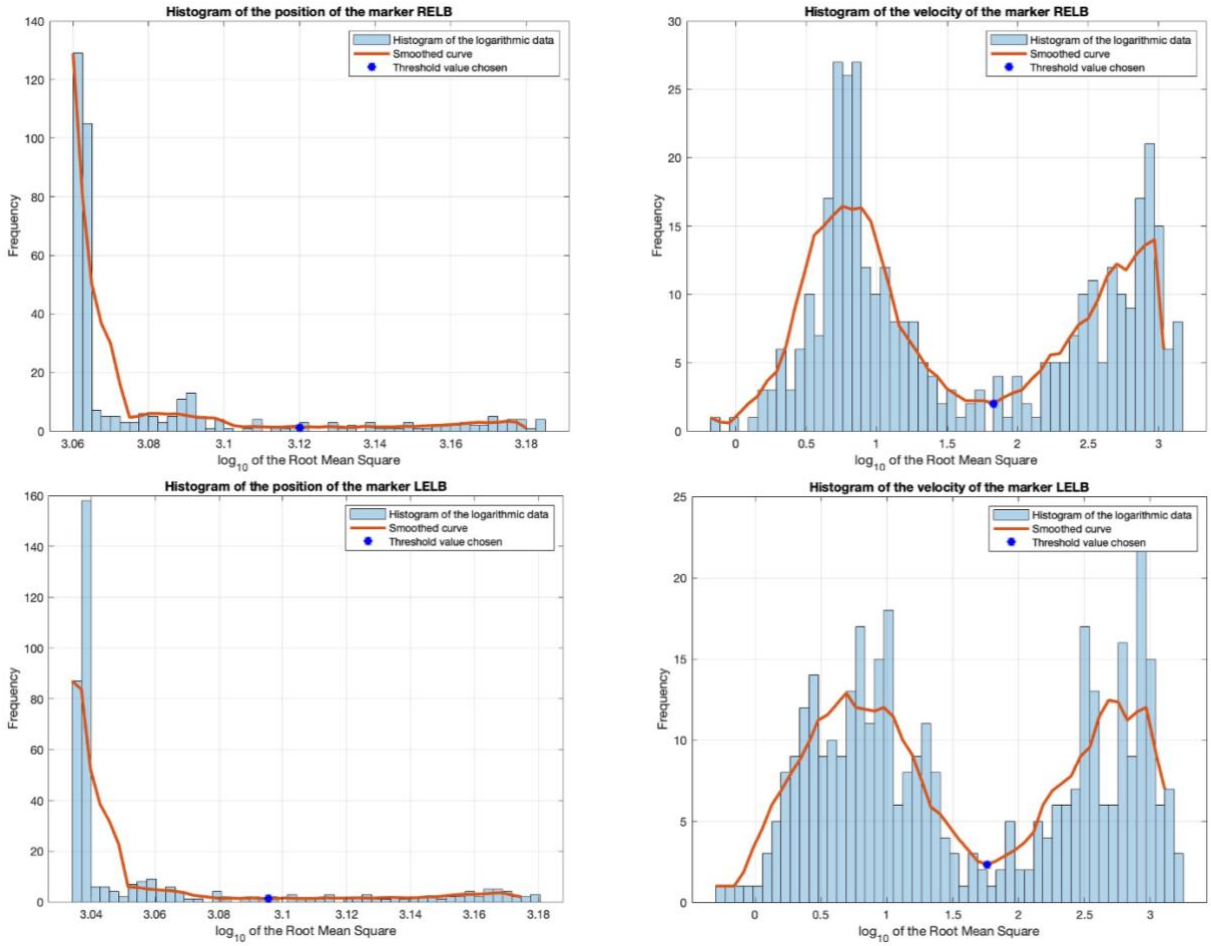

Figure 10. Histograms of the root mean square of position and velocity of markers RELB and LELB in the frontal elevation task in a representative control subject. On the left there the histograms for the base 10 logarithm of the RMS of the position values (up of RELB and down of LELB), while on the right there are the histograms for the base 10 logarithm of the RMS of the velocity values (up for RELB and down for LELB).

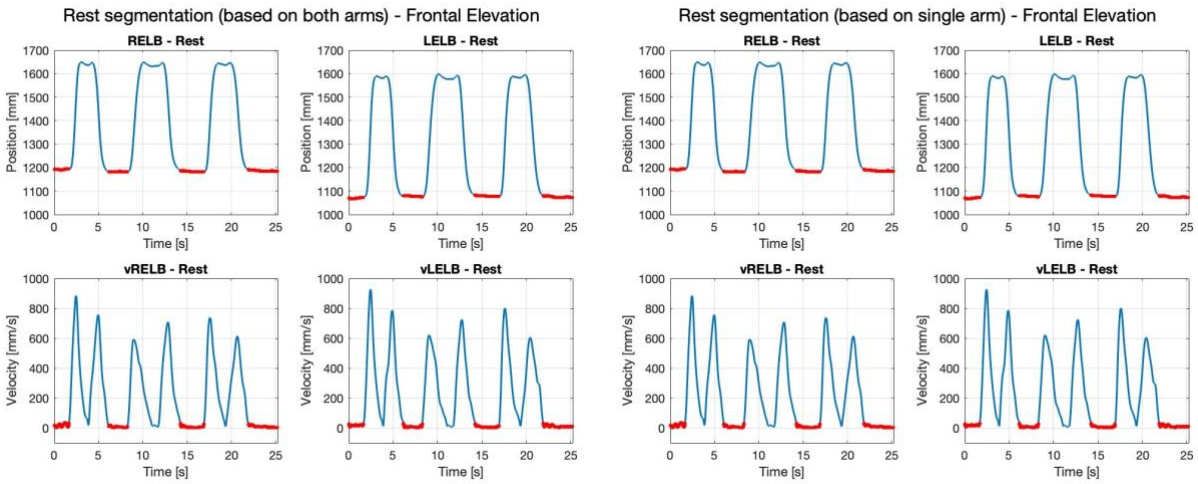

Figure 11. Instants of rest resulting from the segmentation of the movements done both individually on each arm (on the left) and on both arms simultaneously (on the right) in the frontal elevation task in a representative control subject.

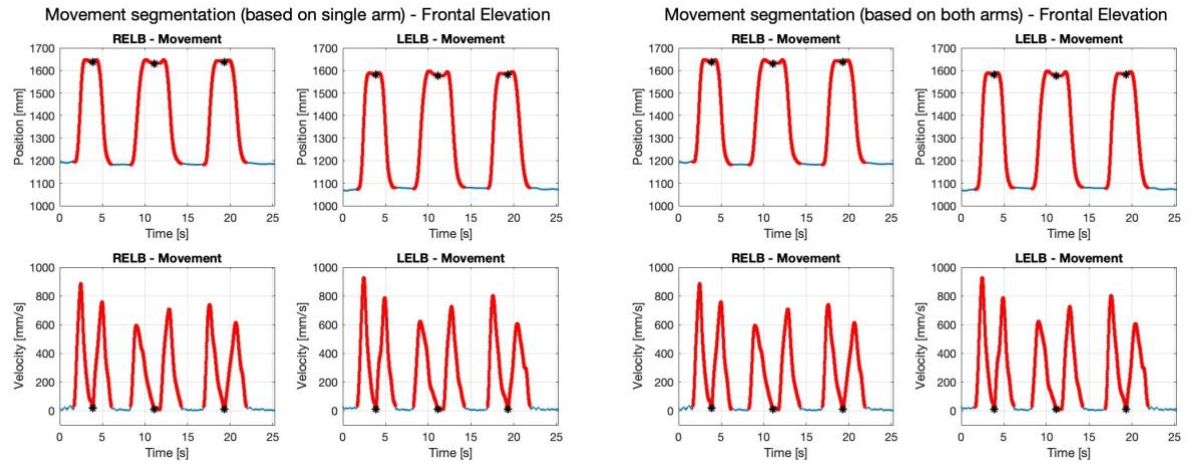

Figure 12. Highlighted Instants of movement and of maximum amplitude reaching obtained with the segmentation of the movements done both individually on each arm (on the left) and on both arms simultaneously (on the right) in the frontal elevation task in a representative control subject.

2.2 **Arms' path evaluation**

In stroke patients, post-stroke arm movements often exhibit disruptions, including slow and asymmetrical speed profiles, and spatial and temporal fragmentation of movement, leading to disturbed hand paths and arm postures [13]. The primary research question sought to investigate whether stroke patients, compared to healthy controls, exhibit differences in the spatiotemporal integration of motion during 3D reaching towards visual targets, as measured by hand path and arm posture features. The study involved eight healthy individuals and sixteen right-hemiparetic stroke patients, with upper limb motion in 3D recorded using a three-camera

optoelectronic system. Reflective markers were attached to bony landmarks of the right arm, and participants were instructed to perform reaching movements towards visual targets. Spatial (hand path and arm posture) and temporal (speed) parameters were measured, revealing significant differences between stroke patients and healthy controls. Specifically, 3D reaching in stroke patients differed significantly from healthy controls, particularly when reaching towards targets in the left direction, suggesting potential influences of target position and distance in extracorporeal space. In patients after stroke evaluating upper limb kinematics serves not only diagnostic but also rehabilitative purposes. Post-rehabilitation, patients commonly face challenges in sustaining motivation to utilize the affected limb, impeding its progress. Therefore, employing a wearable sensor system to assess upper limb movements during daily activities can be instrumental in optimizing the rehabilitation program. In a study conducted by Šlajpah et al.[14] , seven post-stroke patients performed activities of daily living (like drinking, preparing a meal, writing a shopping list, and reading a newspaper) to evaluate their upper limb movement capabilities. The analysis encompassed various kinematic parameters, including the lengths of traveled paths. The findings highlighted that individuals with more pronounced impairment displayed significant movement asymmetry, with the unaffected arm demonstrating movements covering a longer path compared to the affected one. Conversely, those with milder impairment exhibited less asymmetry.

As demonstrated in the study conducted by Mazzarella et al. [15], spatiotemporal parameters such as movement length and execution speed prove to be valuable tools in the kinematic analysis of the upper limb, facilitating both intra- and inter-individual comparisons. Employing a 3D motion capture system, their research focused on collecting data during upper limb movements in infants diagnosed with perinatal stroke (PS), particularly emphasizing pre-reaching movements. During the recording process, retroreflective markers were strategically placed on the infants to capture spatial and temporal variables associated with arm movements. Spatial variables, including movement length, length of the hand path, and straightness ratio, were meticulously measured, alongside temporal variables such as movement speed, movement frequency, and reach frequency. The primary objective of their research was to evaluate the feasibility of employing 3D motion capture to discern differences in movement characteristics among diagnostic groups. This endeavor aimed to significantly contribute to the identification and understanding of motor impairments in at-risk infants through the application of advanced motion capture technology.

Building on the insights gained from these studies, an algorithm has been developed to compute the arm's path length (using markers LELB and RELB) during the functional task,

both in individual directions and as a cumulative measure. Additionally, the algorithm determines the velocity of the movement and the overall duration of the entire movement. Here's an overview of how it operates.

Within the algorithm, the path length calculation takes place within a for loop, iterating over indices corresponding to each movement phase for every repetition of the analyzed functional task. Within this loop, the path length is initially computed along each direction (x, y, z) individually by summing the differences in position between an instant and the previous instant (Equation 4).

$$\Delta x = \sum_i x_{i+1} - x_i \qquad \Delta y = \sum_i y_{i+1} - y \qquad \Delta z = \sum_i z_{i+1} - z_i$$

Equation 4. Path length along each direction. Here i is the i-th component of the marker's data.

Subsequently, the total path length is determined as the vector sum of the lengths obtained in the three directions (Equation 5).

$$\text{path length [mm]} = \sqrt{\Delta x^2 + \Delta y^2 + \Delta z^2}$$

Equation 5. Total path length.

Following the determination of the path length, the duration of each movement repetition is computed, representing the difference between its ending and starting instants (Equation 6).

$$\text{duration of the repetition [s]} = t_e - t_s$$

Equation 6. Duration of a repetition of the functional task. Here t_e is the ending instant, while t_s is the starting instant of the reptition considered.

With both the total path length and movement duration in hand, the velocity is calculated straightforwardly as the ratio between the path length and the duration of the movement (Equation 7).

$$\text{velocity [mm/s]} = \frac{\text{path length}}{\text{duration of the repetition}}$$

Equation 7. Velocity of execution of the repetition.

In this scenario as well, all the obtained parameters are stored for subsequent analysis. The structure of the algorithm is based on a switch construct that addresses three distinct scenarios: movements executed solely with the left arm, movements executed solely with the right arm, and movements executed with both arms. In the first two cases, the parameters are calculated exclusively for one arm, while in the latter case, they are evaluated for both arms.

2.3 **Assessment of shoulders' displacement**

Analyzing shoulder displacement can provide insights into the trunk's role in upper limb motion. This concept is inspired by a study investigating the impact of increased reaching speed on hand kinematics and arm-trunk coordination in stroke-induced hemiplegia patients [16]. The study hypothesized that increased speed might lead to inappropriate compensatory motor responses. During the experimental phase of this study patients with spastic hemiparesis were instructed to do different reaching tasks in two conditions: free trunk and constrained trunk. While doing the functional tasks, a 3-dimensional motion analysis system tracked reflective markers on the finger, wrist, elbow, acromion, and sternum. Regarding trunk displacement measurement, the study highlighted that the contribution of the trunk to reaching movement was assessed using the 3D displacement of the marker placed on the sternum (indicative of trunk flexion-extension) and the marker on the acromion (indicative of a combination of trunk and scapula rotations). The displacement was computed as the distance of the markers between the beginning and end of the movement. Results indicated that patients could voluntarily enhance reaching velocity. In the trunk-free condition with faster speed, elbow extension velocity increased, but elbow extension amplitude decreased, and trunk movement increased. Trunk restraint did not result in decreased elbow extension amplitude with faster speed. Some patients adjusted elbow extension based on reach distance, while others increased trunk compensation with heightened task constraints. The study emphasized that upper limb motor control impairment in stroke patients often involves compensatory trunk flexion to overcome elbow extension limitations. However, faster speed may prompt the use of compensatory strategies.

For the purpose of this thesis, the evaluation of shoulder displacement involves an analysis of the LSHO and RSHO markers, strategically positioned on the left and right acromion, respectively, as well as the segment connecting them. Specifically, the quantification of displacement is expressed in terms of surface area, calculated within the transverse plane (xy plane). This area is delineated between the initial position of the LSHO-RSHO segment and its location when the subject reaches the point of maximum amplitude during the execution of the functional task. The choice of the xy plane is justified by its ability to capture movements of greater magnitude compared to other planes. In fact it catches the forward-backward and lateral movements of the trunk.

The algorithm's implementation encompasses the recording of coordinates for the LSHO and RSHO markers at the initiation of the movement and at the moment the subject achieves maximum amplitude. These recorded coordinates form the vertices of a polygon, and the

subsequent calculation of its area is integral to the analysis. The sides of this polygon are defined by the initial and final positions of the LSHO-RSHO segment, the segment connecting the initial position of LSHO with its final position, and the segment linking the RSHO position with its final location (Figure 13). Utilizing these four vertices, the polygon effectively outlines the spatial footprint of shoulder displacement during the specified task. The Matlab *polyarea* function is then employed to precisely compute the enclosed surface area within this polygon. This function operates by taking the coordinates of the polygon's vertices as input and subsequently calculating the area of the enclosed region within the transverse (xy) plane. This approach proves particularly effective in calculating the area of irregularly shaped polygons, thereby facilitating a nuanced analysis of shoulder displacement during the specified functional task.

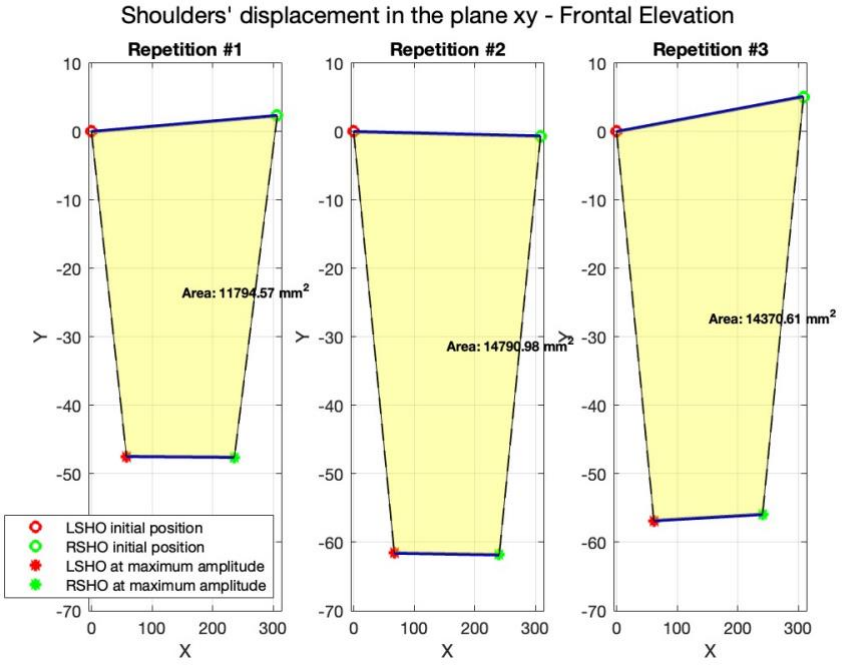

Figure 13. Example of surface area computed for evaluating the displacement of the segment that links the markers LSHO and RSHO in the plane xy.

2.4 Evaluation of circumduction tasks trajectories in the laboratory and the thorax coordinate systems

The thesis written by Monga P. [17] explores the three-dimensional movement patterns of asymptomatic shoulders, shoulders with anterior instability, and the impact of surgical stabilization on these movements. The study reveals differences in movement characteristics between individuals without shoulder issues (control subjects) and those with anterior instability. Data were collected by a motion capture system with reflective markers placed on the upper portion of the body. Participants were instructed to perform four specific movement

tasks: an abduction in the coronal plane, an abduction in the scapular plane, a forward elevation, and a circumduction. Joint angles during abduction, abduction in the scapular plane, and forward flexion were plotted against time and normalized for comparability between the subjects. While, for the analysis of the circumduction movement, the trajectory followed by the elbow was plotted in the sagittal plane. This trace was referenced both to the laboratory system and to the subject's trunk because the circumduction trace obtained with the first reference frame represents non only the movement at the shoulder complex, but also the compensatory trunk movements. In fact, Monga observed that when looking at the trajectories in the laboratory reference frame, both patients and controls displayed almost circular shapes. However, when examining traces in the trunk reference frame (Figure 14), differences between the two groups emerged. To quantify this, Monga computed the area enclosed by the trace using the trapezium rule, so by dividing the area contained under the superior and under the inferior trace into multiple trapeziums and then by subtracting the latter from the former (Figure 15). Analysis of these areas revealed that patients with shoulder instability, in the trunk reference system, produced traces with a smaller area (55.37%) compared to controls. This indicates that shoulder instability affects movement and compensatory trunk changes are responsible for differences not easily noticeable when examining shoulder movements alone in the laboratory reference frame. Therefore, the resultant movement is obtained by a combination of trunk and shoulder movements and the differences between the two groups become evident only when isolating trunk movement, because the trunk motion serves as compensation for limitations in shoulder joint mobility caused by pathology.

So, in alignment with Monga's thesis, for the circumduction tasks the area enclosed by the trajectory has been evaluated relative to both the laboratory reference frame and the thorax reference frame (Figure 16).

To calculate the area, the first step involves establishing the thorax coordinate system which was done in Matlab according to the Vicon Plug-in-Gait model for the thorax [10]. This model relies on markers labelled as CLAV, C7, STRN and T10 (Figure 7), and involves determining the following landmarks: the midpoint between CLAV and C7 (*Thorax Prox*), and the midpoint between STRN and T10 (*Thorax Dist*) (Equation 8).

$$\text{Thorax Prox} = \frac{\text{CLAV} + \text{C7}}{2} \qquad \text{Thorax Dist} = \frac{\text{STRN} + \text{T10}}{2}$$

Equation 8. Thorax landmarks utilized for the creation of the thorax coordinate system.

The origin is then set in *Thorax Prox* and the x, y, z axes directions are calculated based on these landmarks. The z-axis aligns with the direction from *Thorax Dist* to *Thorax Prox*, pointing upwards (Equation 9).

$$\vec{\mathrm{K}}(\mathrm{i}) = \frac{\mathrm{Thorax\ Prox\ (i)} - \mathrm{Thorax\ Dist(i)}}{\|\mathrm{Thorax\ Prox(i)} - \mathrm{Thorax\ Dist(i)}\|}$$

Equation 9. $\vec{\mathrm{K}}$ is the unitary vector that represents the direction of the z-axis, and i is the i-th component of *Thorax Prox* and *Thorax Dist*.

The x-axis direction is determined by the cross product of the unit vector from C7 to CLAV and the z-axis (Equation 10).

$$\overrightarrow{\mathrm{PROV}}(\mathrm{i}) = \frac{\mathrm{CLAV(i)} - \mathrm{C7(i)}}{\|\mathrm{CLAV(i)} - \mathrm{C7(i)}\|} \qquad \vec{\mathrm{I}}(\mathrm{i}) = \frac{\overrightarrow{\mathrm{PROV}}(\mathrm{i}) \times \vec{\mathrm{K}}(\mathrm{i})}{\|\overrightarrow{\mathrm{PROV}}(\mathrm{i}) \times \vec{\mathrm{K}}(\mathrm{i})\|}$$

Equation 10. $\vec{\mathrm{I}}$ is the unitary vector that represents the direction of the x-axis and $\overrightarrow{\mathbf{PROV}}$ is the unitary vector that goes from the marker C7 to the marker CLAV.

Finally, the y-axis direction is obtained as the cross product of the z and x axes (Equation 11).

$$\vec{\mathrm{J}}(\mathrm{i}) = \frac{\vec{\mathrm{I}}(\mathrm{i}) \times \vec{\mathrm{K}}(\mathrm{i})}{\|\vec{\mathrm{I}}(\mathrm{i}) \times \vec{\mathrm{K}}(\mathrm{i})\|}$$

Equation 11. $\vec{\mathrm{J}}$ is the unitary vector that represents the direction of the y-axis.

After obtaining the unit vectors of the thorax reference frame, the data of RELB and LELB are computed in this new reference frame.

For each point, the rotation matrix **R** is considered as follows (Equation 12):

$$\mathbf{R} = \begin{bmatrix} \vec{\mathrm{I}}^{\mathrm{T}} \\ \vec{\mathrm{J}}^{\mathrm{T}} \\ \vec{\mathrm{K}}^{\mathrm{T}} \end{bmatrix}$$

Equation 12. Rotation matrix for the coordinates' transformation.

Subsequently, each point P1 in the laboratory reference frame is transformed into a point P2 in the thorax reference frame using the Equation 13:

$$\mathrm{P2} = (\mathbf{R}^{\mathrm{T}} \cdot \mathrm{P1}) - (\mathrm{R}^{\mathrm{T}} \cdot \mathrm{O1}^{\mathrm{T}})$$

Equation 13. Equation to transform points of a generic reference frame 1 into points of a generic reference frame 2. O1 are the coordinates of the origin (*Thorax Prox*) considered at the same instant as P1.

After computing the coordinates of RELB and LELB in the thorax reference frame, for each circumduction task the trajectories in the xy, xz and yz planes are visualized and their enclosed areas are calculated using the trapezium rule.

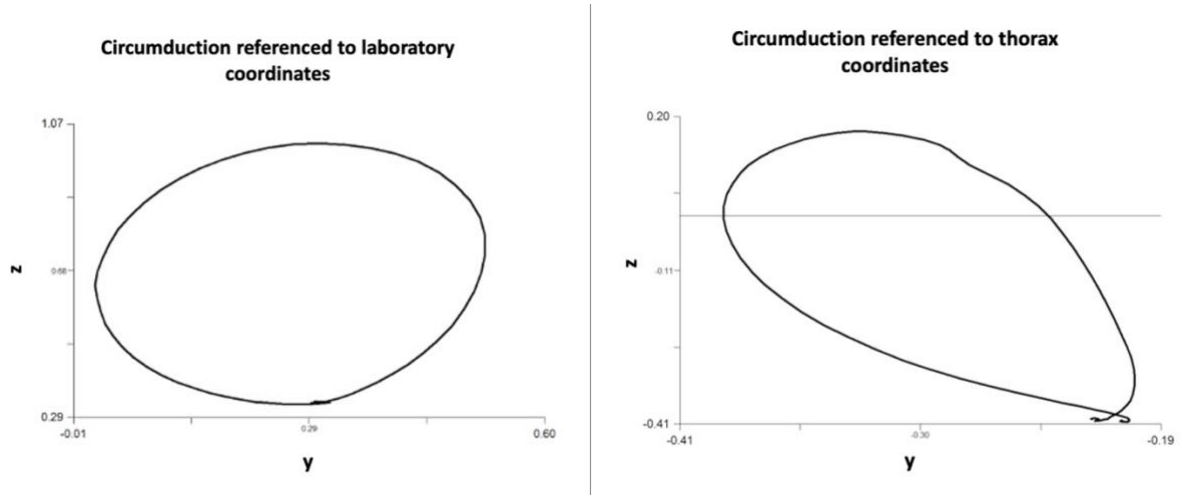

Figure 14. On the left: trajectory of the circumduction movement in the sagittal plane plotted in the laboratory reference frame. On the right: Trajectory of the circumduction movement in the sagittal plane plotted in the trunk reference frame [17].

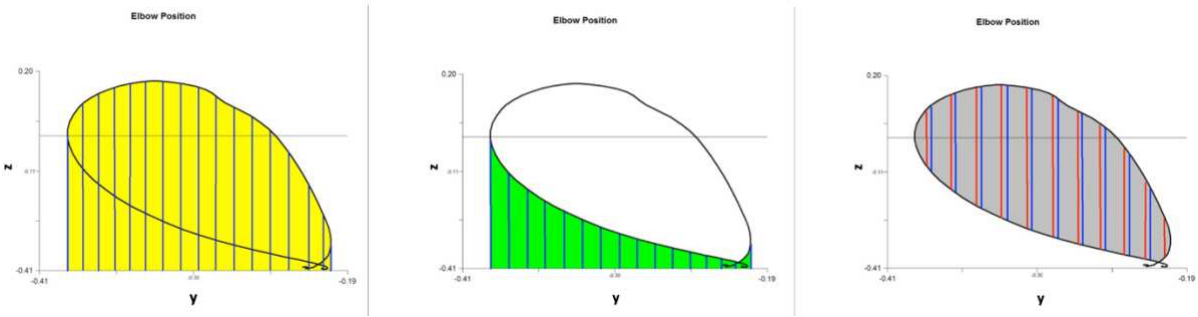

Figure 15. Trapezium rule. Left: area under the superior trace divided into multiple trapeziums. Middle: area under the inferior trace divided into multiple trapeziums. Right: area obtained by subtracting the area under the inferior trace from the area under the superior trace [17].

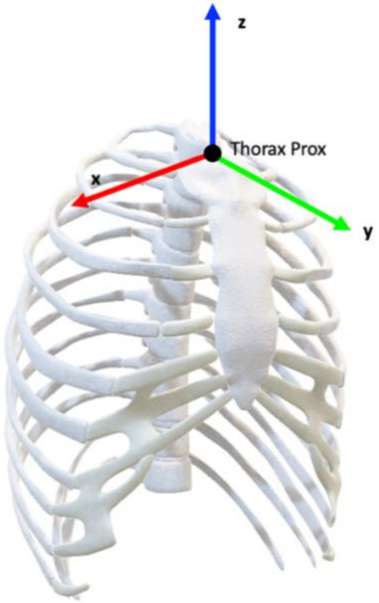

Figure 16. Orientation of the thorax reference frame in the 3D space.

2.5 **Computation of trunk and pelvis joint angles**

It has been demonstrated that trunk and pelvis movements play a role in daily activities that involve upper limb motions. In a recent study by Gates et al. [18], the aim was to characterize and quantify the motions of the shoulder, elbow, wrist, trunk, and pelvis required for eight mono- and bilateral daily tasks. They acquired data using a motion capture system with a set of retroreflective markers placed on the arms, trunk, and pelvis to track the movements of the different body segments. Then they evaluated the range of motion (ROM) of the joint angles. For the trunk and pelvis, motions were evaluated relative to the global coordinate system, and trunk motions relative to the pelvis were also calculated. Results indicated minimal trunk and pelvis movements in most tasks among healthy participants. However, it was hypothesized that individuals with restricted shoulder or elbow joint range of motion might exhibit greater trunk and pelvic angles.

Following this path, several studies have examined trunk and pelvis joint angles in the context of upper limb kinematic differences between healthy individuals and those affected by diseases leading to impairment in one or both upper limbs. In the exploration of upper limb kinematics during daily activities in individuals post-stroke, an increase in trunk angular excursion and path length was observed when tasks were performed with the paretic arm [19]. This compensatory increase aimed to address the decreased range of motion in the shoulder and elbow during upper limb tasks. Participants in this study performed four tasks while seated in front of a table with two bowls (one full of water and one empty) and a spoon. Tasks included reaching and grasping the spoon, reaching with the spoon into the water-filled bowl, scooping water, and pouring it into the empty bowl. Motion data were captured using a set of 21 retroreflective markers and a Vicon Digital system. Joint angles were computed using the Vicon Nexus software based on the Plug-In-Gait model [10]. Here joint excursion was defined as the angle range between the start and the end of each movement.

The interaction between upper body segments during movement has also been explored in children with neuromuscular disorders compared to healthy children [20]. Data collection involved an optical motion capture system tracking retroreflective markers on the upper body. Pelvis angles were computed relative to the global coordinate system, while the trunk was divided into four segments, and angles for each segment were computed relative to the more caudal segment. Pelvis and trunk zero angles were determined during a recording of participants sitting quietly, and joint ROM was defined as the subtraction of the start position angle from the segment angles. Examination of trunk and pelvis ROM during reaching tasks revealed an increase with reaching height, distance, and object weight.

Therefore, it has been chosen to assess compensatory movements of the trunk and pelvis even in the case of subjects affected by upper limb lymphedema. This decision stems from the fact that in individuals with lymphedema, the swelling may impact the normal range of motion in the affected upper limb. Furthermore, this thesis aims to explore potential differences in pelvic and trunk movements in healthy individuals when performing movements with their dominant and non-dominant arm. This comparative analysis can offer a comprehensive understanding of how individuals adjust their movements based on arm dominance.

To calculate the joint angles of the trunk and pelvis, it was crucial to establish both a trunk and a pelvis coordinate system. The trunk reference frame is constructed as illustrated in section 2.4. The pelvis coordinate system is established following the guidelines outlined in the Plug-In Gait guide [10], utilizing the markers placed on the anterior and posterior superior iliac spine (Figure 17). First the landmarks *Asis med* and *Psis med* are computed (Equation 14), the former is the midpoint between the right and left markers located on the anterior superior iliac spine (RASI and LASI), and the latter is the midpoint between the markers on the posterior superior iliac spine (RPSI and LPSI).

$$\text{Asis med} = \frac{\text{RASI} + \text{LASI}}{2}, \qquad \text{Psis med} = \frac{\text{RPSI} + \text{LPSI}}{2}$$

Equation 14. Pelvis landmarks utilized for the creation of the pelvis coordinate system.

Subsequently, the origin of the coordinate system is set at the *Asis med* landmark.

The x-axis direction, representing the dominant axis, is determined by the vector going from the LASI to the RASI marker (Equation 15).

$$\vec{\text{I}}(\text{i}) = \frac{\text{RASI(i)} - \text{LASI(i)}}{\|\text{RASI(i)} - \text{LASI(i)}\|}$$

Equation 15. $\vec{\text{I}}$ is the unitary vector that indicates the direction of the x-axis and i is the i-th component of the markers' data.

The z-axis direction is established as the direction perpendicular to the vector going from the midpoint between the posterior markers to the right anterior marker (Equation 16). Generally, the z-axis points upwards.

$$\overrightarrow{\text{PROV}}(\text{i}) = \frac{\text{RASI(i)} - \text{Psis med(i)}}{\|\text{RASI(i)} - \text{Psis med(i)}\|\text{m}} \qquad \vec{\text{K}}(\text{i}) = \frac{\vec{\text{I}}(\text{i}) \times \overrightarrow{\text{PROV}}(\text{i})}{\left\|\vec{\text{I}}(\text{i}) \times \overrightarrow{\text{PROV}}(\text{i})\right\|}$$

Equation 16. $\vec{\text{K}}$ is the unitary vector indicating the direction of the z-axis, $\overrightarrow{\text{PROV}}$ is the unitary vector that goes from the midpoint between the posterior markers to the RASI marker, and i is the i-th component of the markers' data.

The y-axis direction is then determined as the cross product the other two vectors (Equation 17).

$$\vec{J}(i) = \frac{\vec{K}(i) \times \vec{I}(i)}{\left\|\vec{K}(i) \times \vec{I}(i)\right\|}$$

Equation 17. $\vec{J}$ is the unitary vector of the y-axis direction.

After computing the directions of the x, y, and z axes, the data of RELB and LELB are referenced to the pelvis coordinate system in the same manner used for the trunk reference frame in section 2.4. This involves computing the rotation matrix and applying both axes rotation and origin translation to each data point.

After establishing the two coordinate systems, the computation of joint angles proceeds initially between the trunk and the pelvis, and subsequently between the pelvis and the laboratory coordinate system. The methodology employed for these angle calculations adheres to the approach introduced by Grood and Suntay, since it has been applied by the Standardization and Terminology Committee of the International Society of Biomechanics (ISB) to set standards for most joints in the human body [21]. Grood and Suntay devised a joint coordinate system capable of delineating three-dimensional translational and rotational motion between two rigid bodies. The angular position of a joint is delineated by three distinct angles, each rotating around its corresponding independent rotation axis. In this particular method, flexion-extension occurs about the medial-lateral axis (x-axis), external-internal rotation transpires around the vertical axis (z-axis), and abduction-adduction takes place around the anterior-posterior axis (y-axis) (Figure 18). Positive values are assigned to flexion, abduction, and counterclockwise rotation.

To compute these angles, the algorithm considers matrices (**Ref1** and **Ref2**) defining the coordinate systems for each sample (Equation 18). The matrix **Ref1** defines the coordinate system relative to which the joint angles are computed, while **Ref2** defines the coordinate system of which the angles are calculated.

$$\mathbf{Ref1} = \left[\vec{I}(t) \quad \vec{J}(t) \quad \vec{K}(t)\right] \qquad \mathbf{Ref2} = \left[\vec{\imath}(t) \quad \vec{\jmath}(t) \quad \vec{k}(t)\right]$$

Equation 18. Definition of the two matrices which define the two coordinate systems of which the joint angles are evaluated. Here $\vec{I}, \vec{J}, \vec{K}, \vec{\imath}, \vec{\jmath},$ and $\vec{k}$ are the unitary vectors defining the directions of the axes of the reference frames Ref1 and Ref2, and t is the t-ish sample considered.

Given the two coordinate systems, it computes the rotation matrix $\mathbf{R}_t$ given by their combination (Equation 19).

$$\mathbf{R}_t = \begin{bmatrix} \vec{I}^T(t) \cdot \vec{\imath}(t) & \vec{J}^T(t) \cdot \vec{\imath}(t) & \vec{K}^T(t) \cdot \vec{\imath}(t) \\ \vec{I}^T(t) \cdot \vec{\jmath}(t) & \vec{J}^T(t) \cdot \vec{\jmath}(t) & \vec{K}^T(t) \cdot \vec{\jmath}(t) \\ \vec{I}^T(t) \cdot \vec{k}(t) & \vec{J}^T(t) \cdot \vec{k}(t) & \vec{K}^T(t) \cdot \vec{k}(t) \end{bmatrix} = \begin{bmatrix} R_{11}(t) & R_{12}(t) & R_{13}(t) \\ R_{21}(t) & R_{22}(t) & R_{23}(t) \\ R_{31}(t) & R_{32}(t) & R_{33}(t) \end{bmatrix}$$

Equation 19. Rotation matrix obtained combining the two coordinate systems.

Joint angles (α_t, β_t, γ_t) are subsequently determined using the rotation matrix with the Equation 20 obtained by the mathematical description of the Grood-Suntay method[21]:

$$\alpha_t = 180 \cdot \frac{\tan^{-1}\left(\frac{R_{32}(t)}{R_{33}(t)}\right)}{\pi} \qquad \beta_t = 180 \cdot \frac{\sin^{-1}\left(R_{13}(t)\right)}{\pi} \qquad \gamma_t = 180 \cdot \frac{\tan^{-1}\left(\frac{R_{12}(t)}{R_{22}(t)}\right)}{\pi}$$

Equation 20. Equations for computing the flexion-extension, abduction-adduction and rotation angles, respectively.

When considering the angles between the trunk and pelvis, they elucidate the dynamic relationship between these segments. The flexion-extension angle (α_t) provides information about the forward and backward movements of the trunk in relation to the pelvis. A positive value indicates flexion, or forward bending, while a negative value signifies extension, or backward straightening. The abduction-adduction angle (β_t) sheds light on the lateral movements of the trunk concerning the pelvis. A positive value corresponds to a lateral bending towards the left, while a negative value denotes a lateral bending towards the right. Furthermore, the rotation angle (γ_t) captures the twisting or rotational movements of the trunk relative to the pelvis. A positive value indicates counterclockwise rotation, while a negative value signifies clockwise rotation.

Moving on to the angles between the pelvis and the laboratory coordinate system, these measurements elucidate the orientation of pelvic movements within the overall laboratory framework. The flexion-extension angle (α_t) in this context describes the pelvic inclination, indicating whether the pelvis is tilting forward (flexion, positive) or backward (extension, negative). The abduction-adduction angle (β_t) in the pelvis-laboratory relationship signifies lateral tilting of the pelvis within the laboratory plane. A positive value indicates tilting towards the left (right side down), while a negative value signifies tilting towards the right (left side down). Lastly, the rotation angle (γ_t) in the pelvis context reveals the rotational orientation of the pelvis within the laboratory coordinate system. A positive value corresponds to counterclockwise rotation, while a negative value indicates clockwise rotation.

Finally, for each joint angle in each functional task, the algorithm computes the mean value at rest and subtracts it to obtain only the displacement from the rest position (Figure 19).

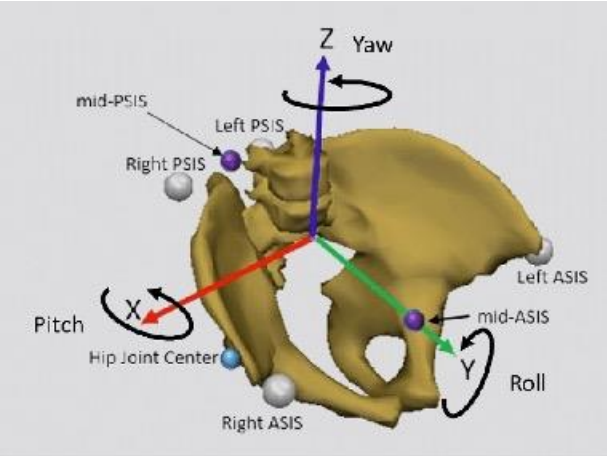

Figure 17. Orientation of the pelvis reference frame in the 3D space.

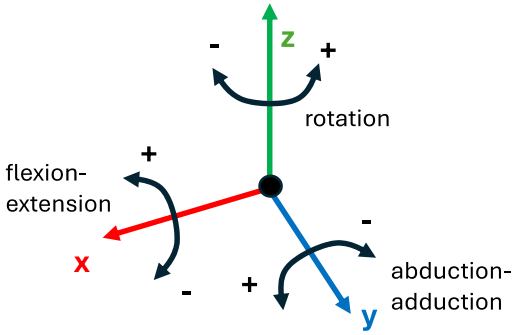

Figure 18. Joint angles defined by rotations occurring about the three joint coordinate axes.

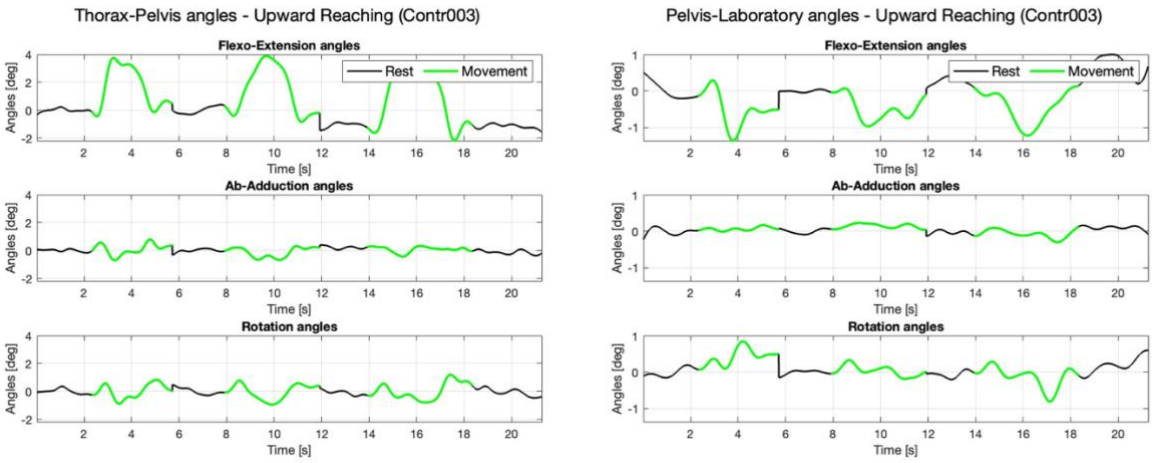

Figure 19. Visualization of the thorax-pelvis (on the left) and pelvis-laboratory (on the right) joint angles computed for a representative control subject in the upward reaching task.

2.6 **Statistical analysis**

In this thesis, a statistical analysis was conducted to compare the laterality in controls using Matlab. Specifically, a paired Wilcoxon test was employed, with a predetermined significance level of 0.05. The Wilcoxon test, also referred to as the Wilcoxon signed-rank test, is a non-parametric method utilized to assess whether there is a significant difference between two related samples or paired observations. It does not assume normal distribution, making it suitable for small sample sizes or when data distribution is not known. The analysis focused on comparing various metrics between the dominant and non-dominant arms, including path length, velocity, displacement of the LSHO-RSHO segment, and differences in trajectory area between the laboratory and the thorax coordinate systems, along with angular excursion. This comprehensive comparison allowed for the discernment of any noteworthy disparities in performance between the two arms, providing valuable insights into the influence of laterality on the measured parameters.

3.
RESULTS

3.1 **Upper limb kinematics**

The examination of upper limb kinematics during functional tasks involves a comprehensive assessment of both the overall path length and the execution velocity of individual movements. To conduct this analysis, mean values for both path length and velocity are calculated for each subject. The resulting means are then visually depicted using a boxplot for control subjects and a scatter plot for the two patients (Figure 20, Figure 21, Figure 22, and Figure 23). Path length is measured in millimetres [mm], while velocity is measured in millimetres per second [mm/s]. Within each diagram, a comparison is drawn between the values recorded for the dominant and non-dominant arms (for control subjects) and between the arm unaffected by lymphedema and the affected arm (for the patients). This graphical representation serves to enhance our comprehension of how upper limb kinematics vary across different tasks and conditions, offering valuable insights into the complexities of functional movements in both healthy individuals and those with lymphedema.

In assessing upper limb symmetry, it is beneficial to examine variations in values between the two arms (dominant and non-dominant, or affected and unaffected). Specifically, variations in path length and velocity are considered for tasks performed with one arm at a time, as tasks executed simultaneously with both arms typically show minimal discrepancies in path length and velocity (Figure 20, Figure 21, Figure 22, and Figure 23). Variations are determined by subtracting the results of the non-dominant or affected arm from those of the dominant or unaffected arm. The resulting variations between the two arms are then visually depicted using a boxplot for control subjects and a scatter plot for the two patients (Figure 24 and Figure 25).

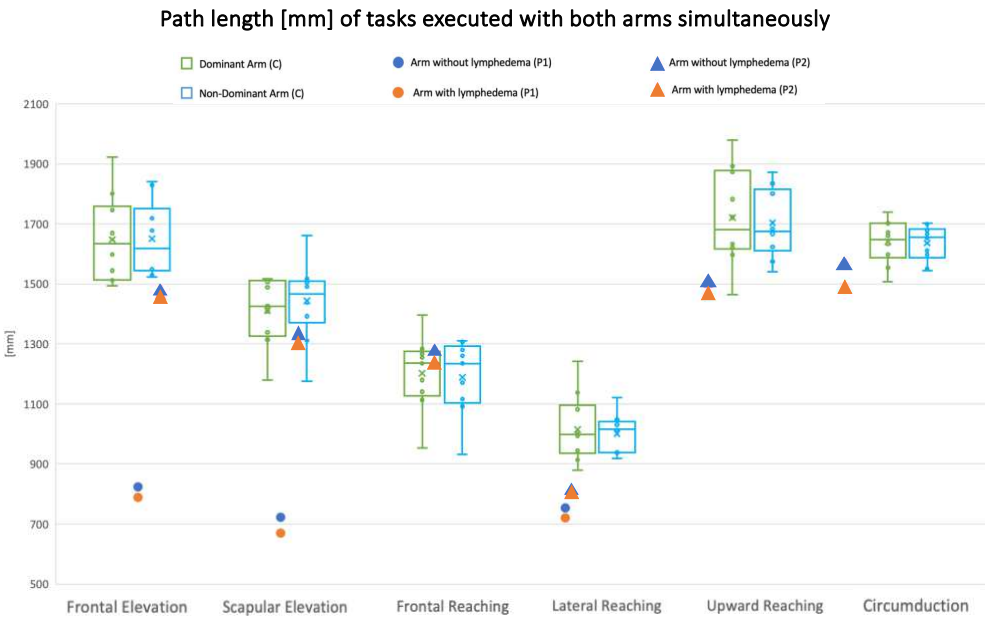

Figure 20. Diagram displaying the outcomes obtained from the comprehensive assessment of overall path length in functional tasks executed with both arms simultaneously. The mean path length values are calculated for each subject across multiple repetitions of the movement in every task. For control subjects (C), results are categorized into those achieved with the dominant arm and the non-dominant arm. In contrast, for patients (P1 and P2), the distinction is made between values attained with the upper limb unaffected by lymphedema and the one affected by it. All measurements presented in the diagrams are expressed in millimeters [mm]. It must be considered that the patient Lymphedema001 (here labelled as P1) has executed with both arms only the frontal elevation, the scapular elevation, and the lateral reaching tasks.

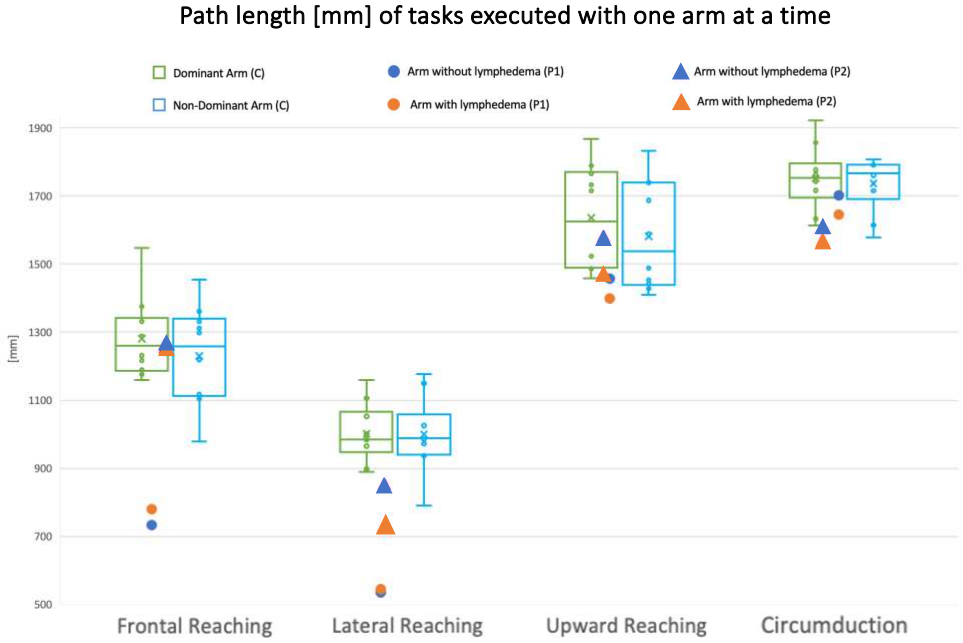

Figure 21. Diagram displaying the outcomes obtained from the comprehensive assessment of overall path length in functional tasks executed with one arm at a time. In analyzing the data, the mean path length

values are calculated for each subject across multiple repetitions of the movement in every task. For control subjects (C), results are categorized into those achieved with the dominant arm and the non-dominant arm. In contrast, for patients (P1 and P2), the distinction is made between values attained with the upper limb unaffected by lymphedema and the one affected by it. All measurements presented in the diagrams are expressed in millimeters [mm]. Here P1 is the patient Lymphedema001, while P2 is the patient Lymphedema002.

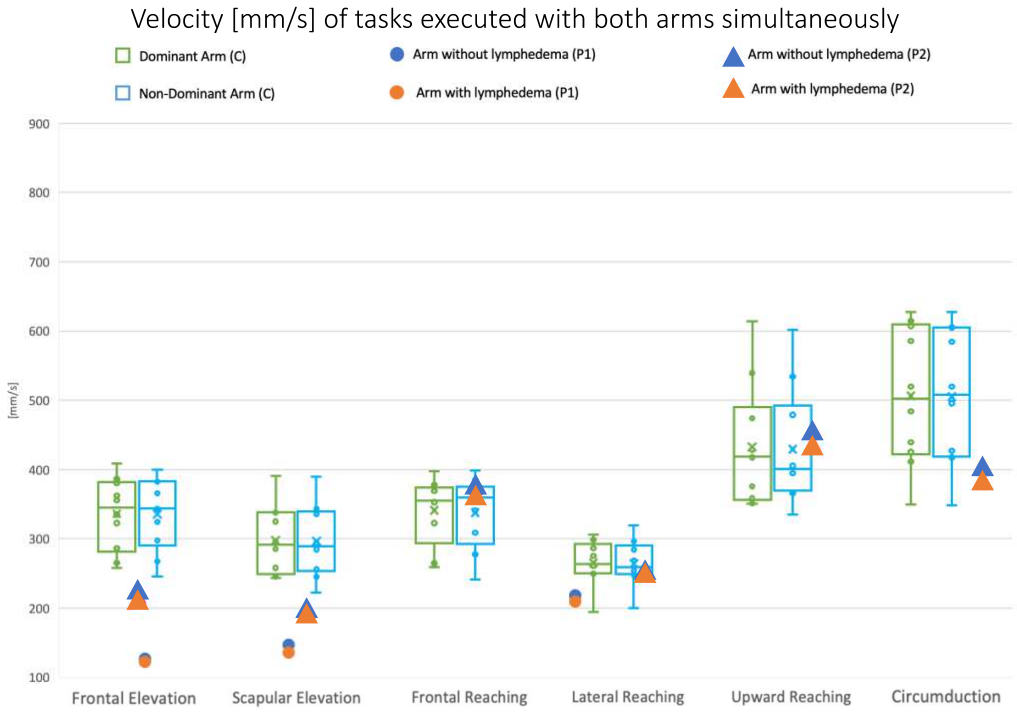

Figure 22. Diagram displaying the outcomes obtained from the comprehensive assessment of velocity in functional tasks executed with both arms simultaneously. In analyzing the data, the mean velocity values are calculated for each subject across multiple repetitions of the movement in every task. For control subjects (C), results are categorized into those achieved with the dominant arm and the non-dominant arm. In contrast, for patients (P1 and P2), the distinction is made between values attained with the upper limb unaffected by lymphedema and the one affected by it. All measurements presented in the diagrams are expressed in millimeters per second [mm/s]. It must be considered that the patient Lymphedema001 (here labelled as P1) has executed with both arms only the frontal elevation, the scapular elevation, and the lateral reaching tasks.

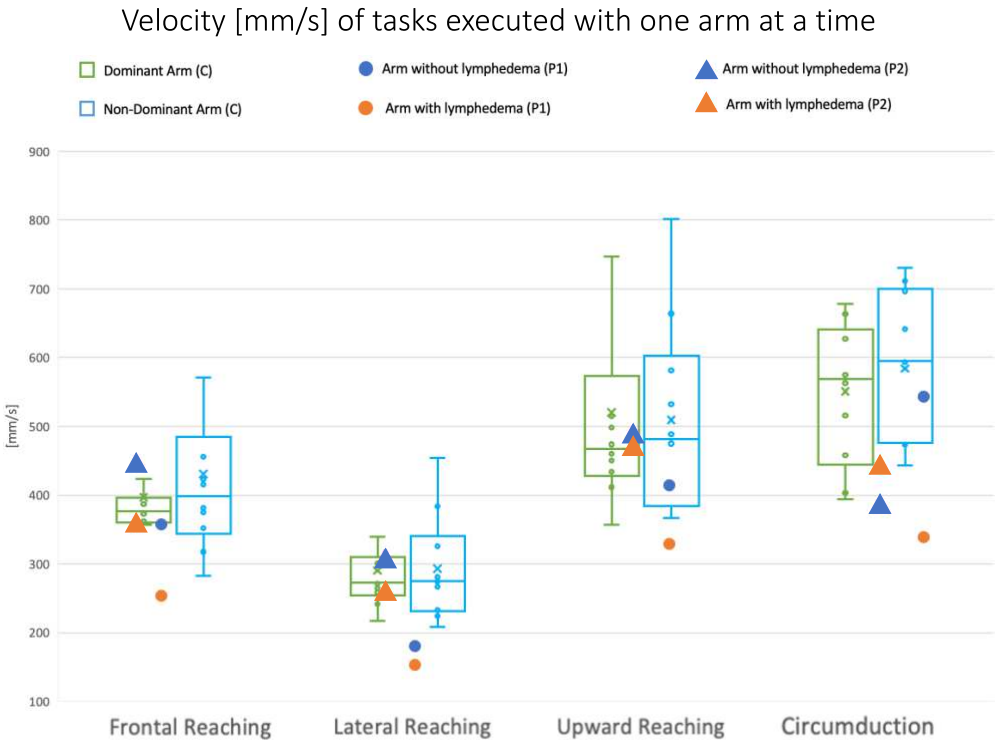

Figure 23. Diagram displaying the outcomes obtained from the comprehensive assessment of velocity in functional tasks executed with one arm at a time. In analyzing the data, the mean velocity values are calculated for each subject across multiple repetitions of the movement in every task. For control subjects (C), results are categorized into those achieved with the dominant arm and the non-dominant arm. In contrast, for patients (P1 and P2), the distinction is made between values attained with the upper limb unaffected by lymphedema and the one affected by it. All measurements presented in the diagrams are expressed in millimeters per second [mm/s]. Here P1 is the patient Lymphedema001, while P2 is the patient Lymphedema002.

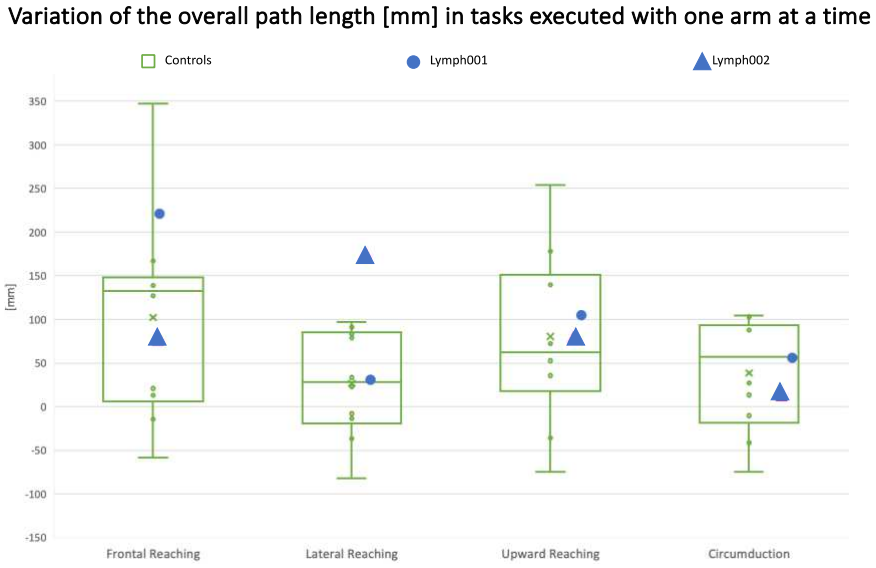

Figure 24. The variation in path length values between the two upper limbs is analyzed during functional tasks performed with one arm at a time. For control subjects, this variation is computed by subtracting the

values obtained for the dominant arm from those obtained for the non-dominant arm. Conversely, for patients, it is calculated by subtracting the values for the arm unaffected by lymphedema from those for the affected one. A positive variation indicates that the path executed with the dominant or unaffected arm is longer than the one performed with the other upper limb. Conversely, a negative variation suggests that the non-dominant or affected path is longer than the dominant or unaffected one.

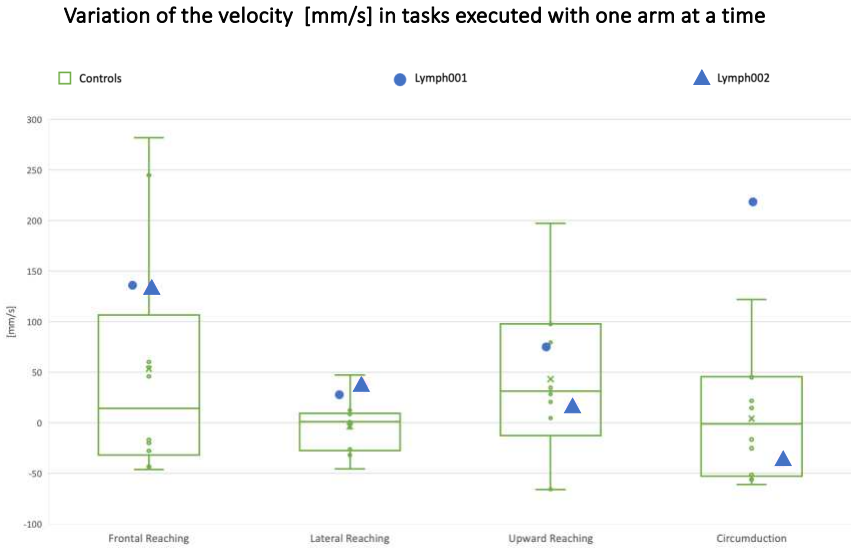

Figure 25. The variation in velocity values between the two upper limbs is analyzed during functional tasks performed with one arm at a time. For control subjects, this variation is computed by subtracting the values obtained for the dominant arm from those obtained for the non-dominant arm. Conversely, for patients, it is calculated by subtracting the values for the arm unaffected by lymphedema from those for the affected one. A positive variation indicates that the functional task is executed faster with the dominant or unaffected arm than the one performed with the other upper limb. Conversely, a negative variation suggests that the non-dominant or affected movement is faster than the dominant or unaffected one.

3.1.1 *Comparison between the dominant and the non-dominant arms*

When examining the diagrams depicting the mean path length values for each arm in various functional tasks (Figure 20 and Figure 21), no discernible differences are evident. Inspecting the diagrams illustrating the variation in path length between the dominant and non-dominant arms (Figure 24) the largest differences emerge particularly in the frontal and upward reaching tasks. Conversely, in the lateral reaching and circumduction tasks, these differences between the upper limbs are less pronounced. Executing a paired Wilcoxon test with a significant p-value <0.05 reveals that the difference in path length between the two arms is significant only in the upward reaching task ($p=0.034$).

Regarding velocity values, it is apparent that velocities for both arms are nearly identical across all tasks performed simultaneously with both arms (Figure 22). However, in tasks

executed with one arm at a time, the discrepancy between the two arms is more noticeable, particularly in the frontal and upward reaching tasks. Furthermore, it is noteworthy that in these functional tasks, the velocity of the non-dominant upper limb exceeds that of the dominant one, as depicted in the velocity diagrams (Figure 23). Despite minimal differences observable in the diagram, when evaluated with a paired Wilcoxon test with a p-value of 0.05, these differences do not appear to be significant.

3.1.2 *Comparison between individuals affected and unaffected by upper limb lymphedema*

In individuals experiencing upper limb lymphedema, in each functional task, the path covered by the arm without lymphedema is consistently longer than that of the affected arm, as depicted in Figure 20 and Figure 21. This contrast is especially noticeable when tasks are performed with one arm at a time, although it is evident in other tasks as well.

Regarding velocity values, it is noteworthy that even though the path taken by the arm affected by lymphedema is shorter, the velocity values are higher for the unaffected arm (Figure 22 and Figure 23), with the exception of patient Lymphedema002 during the circumduction task performed with one arm at a time. This discrepancy arises because, despite the shorter path, the duration of the movement is either similar or longer for the arm affected by lymphedema compared to the movement executed with the unaffected limb (Figure 26).

Finally, comparing the values obtained for the control group with the ones obtained for the patient group it is visible that the second group achieves in terms of path length values lower than the first group, especially the subject Lymphedema001. This also reflects in the velocity values.

In assessing upper limb symmetry, it is beneficial to compare values between control subjects and patients to discern any differences. This comparison involves examining variations in values between the two arms (dominant and non-dominant, or affected and unaffected). Analyzing the variation in path length between the upper limbs reveals noteworthy findings (Figure 24). For instance, in the case of patient Lymphedema001, the asymmetry between her arms is either nearly similar (in lateral reaching and circumduction) or more pronounced (in frontal and upward reaching) compared to the average asymmetry observed in control subjects. Conversely, for patient Lymphedema002, significant asymmetry between the affected and unaffected upper limbs is primarily evident in the lateral reaching task. However, in upward reaching, the asymmetry is slightly greater than the control group's average, while in frontal reaching and circumduction, the asymmetry is even less than the average observed in control subjects.

Examining the variation in velocity values (Figure 25), it's evident that the asymmetry observed in patient Lymphedema001 surpasses that of the control group across all functional. Conversely, in patient Lymphedema002, while the asymmetry is greater than the control group's average during frontal and lateral reaching tasks, it falls below the control group's average during upward reaching and circumduction tasks.

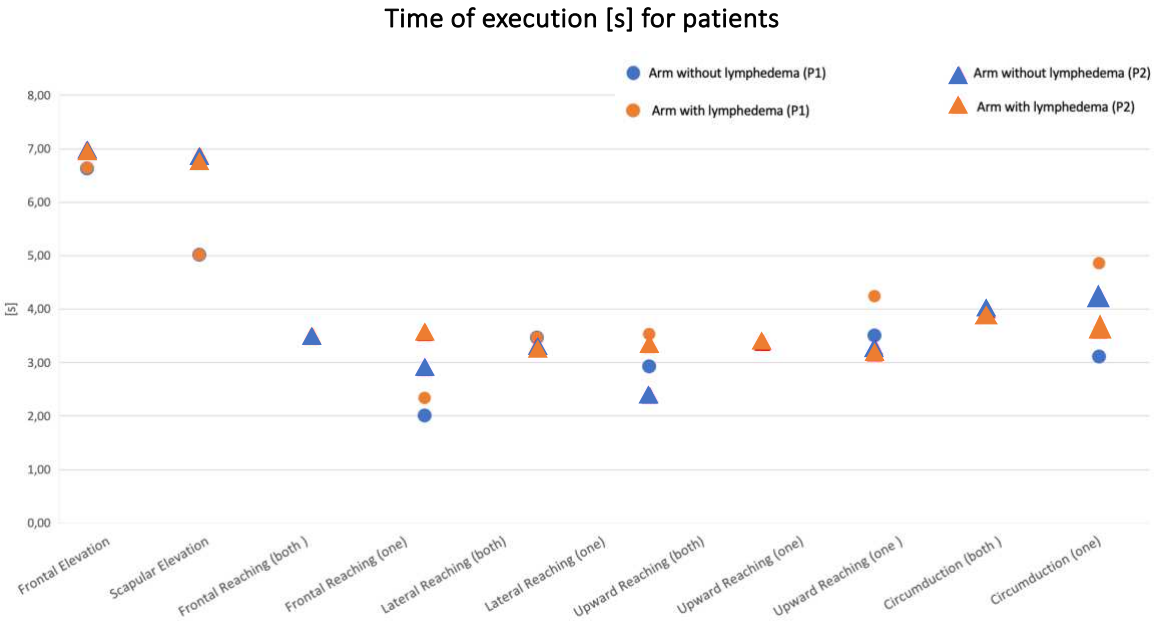

Figure 26. Mean values of the duration of the functional tasks for the two subjects affected by upper limb lymphedema. P1 is the patient Lymphedema001, while P2 is the patient Lymphedema002.

3.2 **Trunk compensation mechanisms**

To assess the extent of involvement of the trunk and pelvis during the execution of upper limb functional tasks, various parameters have been taken into account. Initially, a detailed analysis of shoulder movements was conducted to explore trunk displacement in these tasks. This examination specifically focused on tracking the displacement of the line connecting the acromion of the two shoulders, providing insights into trunk movement in the transverse plane (xy).

For an examination of trunk motion in the sagittal plane (yz), the emphasis shifted to analyzing the amplitude of trajectories during circumduction tasks. This approach allowed for an understanding of changes in amplitude concerning movement referenced to the trunk coordinate system as opposed to the laboratory (global) coordinate system.

Lastly, joint angles between the trunk and pelvis, as well as between the pelvis and the laboratory, were considered. This analysis aimed to elucidate how these joint angles contribute to compensating for the limited mobility of the upper limb.

3.2.1 *Shoulders movement during the upper limb motion*

To examine the shoulder displacement in the xy plane, which serves as an indicator of trunk movement in the corresponding plane, the analysis focused on quantifying the area between the two segments connecting the two markers LSHO and RSHO, on at the initial instant of the movement and the other at the instant of reaching the maximum amplitude. All measurements in this analysis are expressed in square millimetres [mm^2]. For control subjects, the obtained values are presented in a boxplot, showcasing the mean values across task repetitions for each subject. In contrast, for the two patients, the results are illustrated in a scatterplot, featuring the mean values of the repetitions. This approach provides a detailed visualization of the observed metrics, allowing for a comprehensive understanding of shoulder displacement in the xy plane for both control subjects and patients.

Upon reviewing the diagrams depicting tasks performed with both arms simultaneously (Figure 27), a consistent pattern emerges. In all functional tasks, there is a noticeable trend where the displacement of the segment between the left shoulder (LSHO) and right shoulder (RSHO) registers higher values for the patients compared to the mean value observed in the control group. This implies that patients tend to move their trunk more medially in the transverse plane, encompassing backward-forward and lateral movements, when compared to control subjects. Consequently, the compensatory action of the trunk is more prominent in patients undergoing the assessed functional tasks.

When analyzing the diagrams derived from functional tasks performed with one arm at a time (Figure 28), several noteworthy distinctions emerge. In control subjects a clear pattern emerges between the dominant and non-dominant arm. When tasks are executed with the non-dominant arm, there is a noticeable increase in shoulder displacement, and consequently, trunk movement in the xy plane is more pronounced compared to tasks performed with the dominant arm. However, when evaluating these differences with a paired Wilcoxon test with a p-value of 0.05, these do not appear to be significant.

In patients when distinguishing between the arm affected by upper limb lymphedema and the unaffected arm, displacement values are consistently higher when the subject executes the movement with the affected upper limb. This implies that the trunk plays a significant role in compensating for mobility limitations during the motion.

In a comprehensive comparison between control subjects and patients, it becomes clear that the discrepancies in displacement values between different arms are more pronounced within the patient group. Specifically, when examining the variation in displacement of the segment linking LSHO-RSHO during functional tasks performed with one upper limb at a time (Figure 29), it's evident that the asymmetry in trunk displacement between when only the dominant or unaffected arm is in motion and when only the other arm is in motion is more noticeable in the patient group.

Particularly, this asymmetry is consistently greater for patient Lymphedema001 compared to controls, while for patient Lymphedema002, it is more pronounced across all tasks except for the upward reaching task. This highlights the presence of disparities between both sides in both groups, with compensatory trunk movements being more prominent and significant within the patient group.

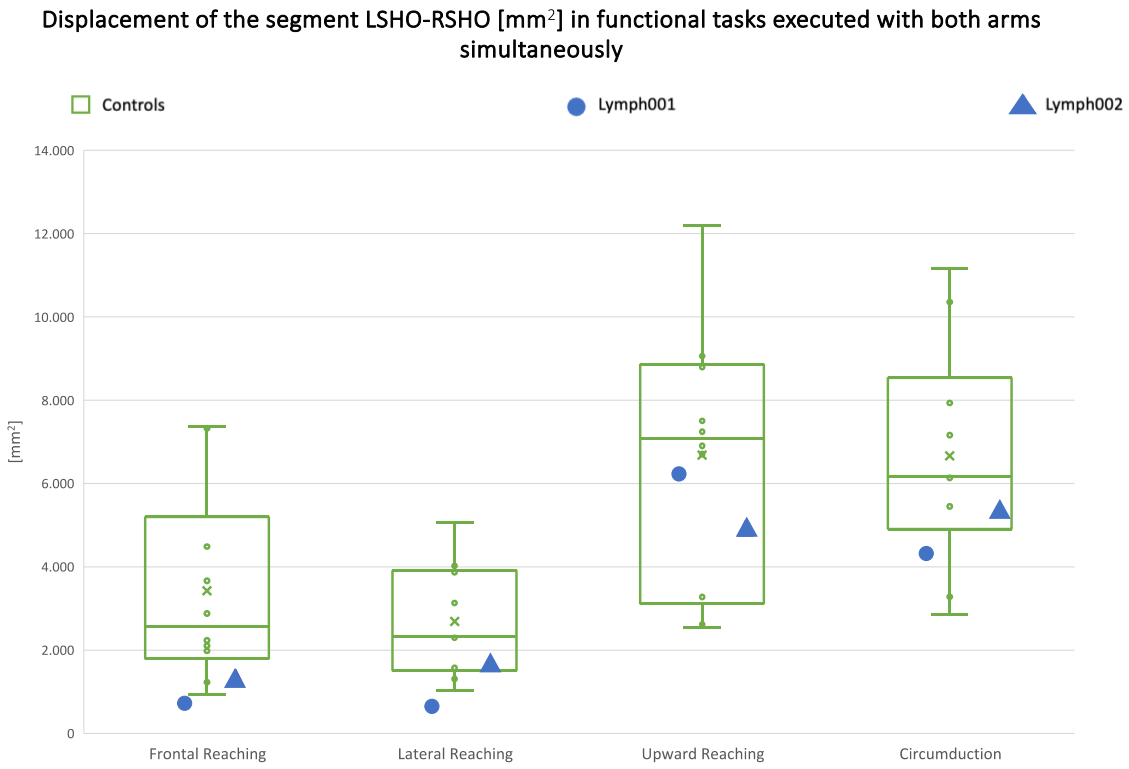

Figure 27. Displacement [mm^2] of the segment linking LSHO-RSHO between the instant of start of the movement and the instant of reaching the maximum amplitude in tasks executed with both arms simultaneously. It must be considered that the patient Lymphedema001 has performed with both arms only the frontal elevation, the scapular elevation, and the lateral reaching tasks.

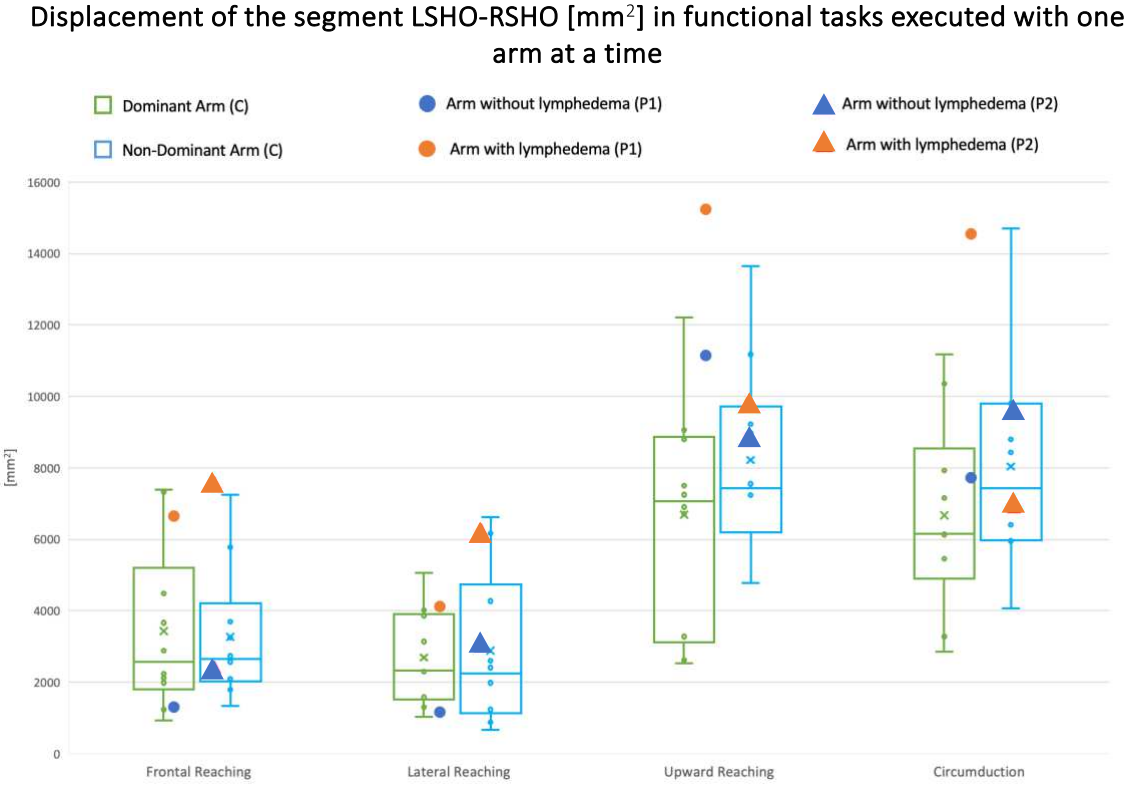

Figure 28. Displacement [mm²] of the segment linking LSHO-RSHO between the instant of start of the movement and the instant of reaching the maximum amplitude in tasks executed with one arm at a time. For control subjects (C), results are categorized into those achieved with the dominant arm and the non-dominant arm. In contrast, for patients (P1 and P2), the distinction is made between values attained with the upper limb unaffected by lymphedema and the one affected by it. Here P1 is the patient Lymphedema001, while P2 is the patient Lymphedema002.

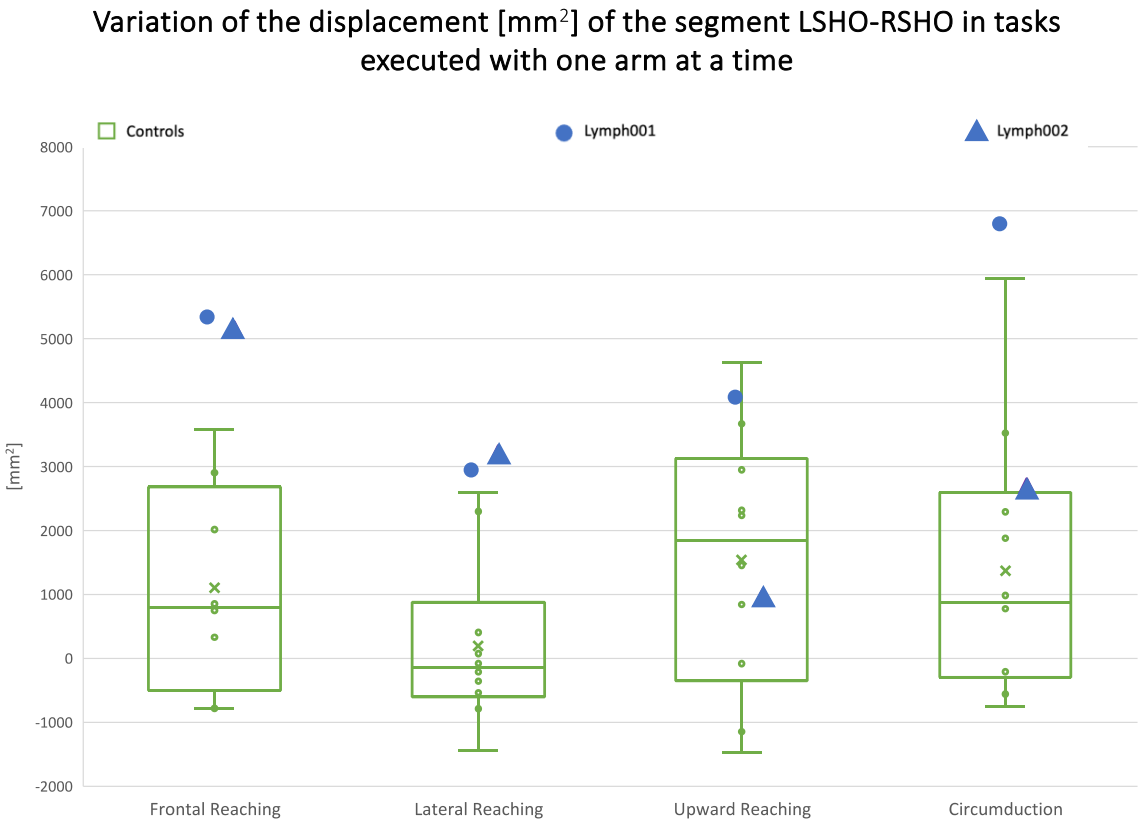

Figure 29. Variation in the displacement of the segment connecting the left shoulder (LSHO) to the right shoulder (RSHO) assessed by comparing the segment displacement when the functional task is carried out with the non-dominant or affected upper limb to the displacement when the task is performed with the opposite arm. If the result is a positive value, there is more displacement of the trunk during the non-dominant or affected upper limb movement. Instead, a negative variation means that the trunk compensatory action is greater when the movement is performed when the dominant or unaffected arm.

3.2.2 *Area of the circumduction tasks trajectories*

To analyze trunk contribution in the sagittal plane, the method proposed by Monga P. [17] was utilized. For circumduction tasks, the area [mm^2] enclosed by the trajectory was evaluated in both the laboratory and thorax reference frames to quantify the influence of the trunk during upper limb motion. For each subject the area for each repetition was computed in both coordinate systems. Subsequently, the mean value of the area was calculated for each system, and the variation between the laboratory coordinate system and the thorax coordinate system has been illustrated (Figure 30) using a boxplot for the control subjects and a scatterplot for the two patients.

In controls it can be noticed that the difference of the two areas is larger for the execution with the non-dominant arm, meaning that the trunk helps in the motion by following the arm's movement, so the trajectory amplitude respect to the laboratory reference frame is bigger than the one respect to the thorax reference frame, where trunk movement is mitigated. This

difference is found to be significant, as determined by the paired Wilcoxon test with a p-value of 0.05, when the task is performed with only one arm at a time (p=0,0078). This phenomenon is also evident in patients; here the difference in trajectory amplitude is more pronounced for the arm affected by lymphedema, indicating increased trunk movement in such cases.

In the methodology outlined in the existing literature, attention is not only directed towards the area of the circumduction trajectory but also towards the trajectory's shape. It has been demonstrated that in healthy individuals, the trajectory shape, relative to both the global and thorax coordinate systems, tends to assume an almost circular form. Moreover, there were no significant differences observed in shape between the trajectories obtained concerning the laboratory and those obtained concerning the trunk. Conversely, in individuals with impaired upper limb mobility, the shapes of the two trajectories exhibit distinctions. They tend to form an almost circular shape concerning the laboratory coordinate system and a more elongated shape concerning the thorax coordinate system. Following this conceptual framework, the trajectories' shapes in the yz plane for all subjects have been analyzed. It becomes apparent that in the control group (Figure 31), the shapes of the trajectories are nearly consistent across subjects in both reference frames. However, it is noteworthy that trajectories concerning the thorax reference frame are comparatively smaller, reflecting the compensatory trunk motion observed in controls, as mentioned earlier. In contrast, for patients (Figure 32), the differences in shape and amplitude of the trajectories are more pronounced, indicating that trunk compensation is more significant than in the control group.

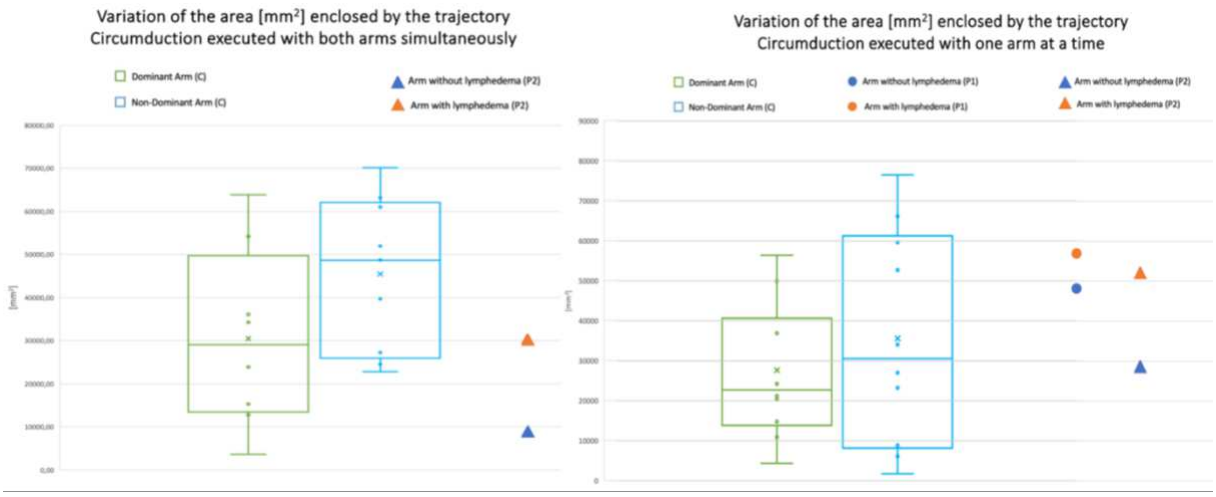

Figure 30. Variation of the area [mm^2] of the trajectory between the laboratory and the thorax reference frames in the circumduction tasks performed with both arms simultaneously (left) and with one arm at a time (right). Here C are the controls, P1 is the patient Lymphedema001, and P2 is the patient Lymphedema002.

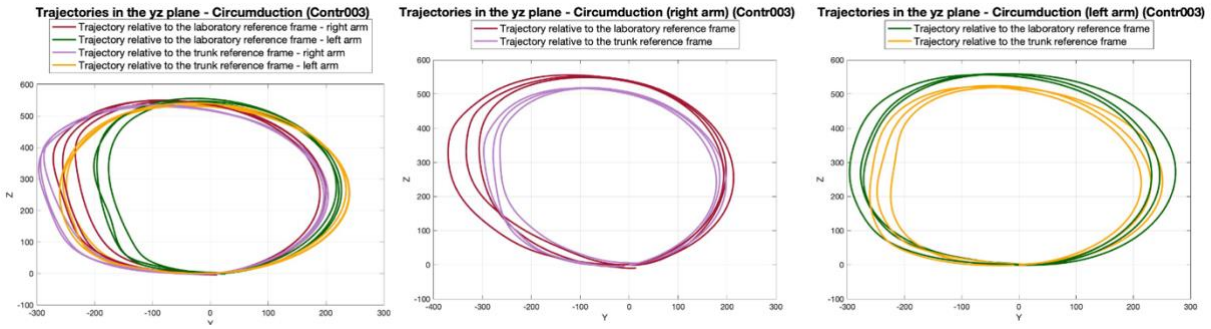

Figure 31. Example of trajectories of the circumduction tasks followed by both arms in control subjects. In the left column there is the trajectory of the circumduction task executed with both arms simultaneously, in the middle column there is the trajectory of the circumduction task executed with the dominant arm, and in the right column there is the trajectory of the circumduction task executed with the non-dominant arm.

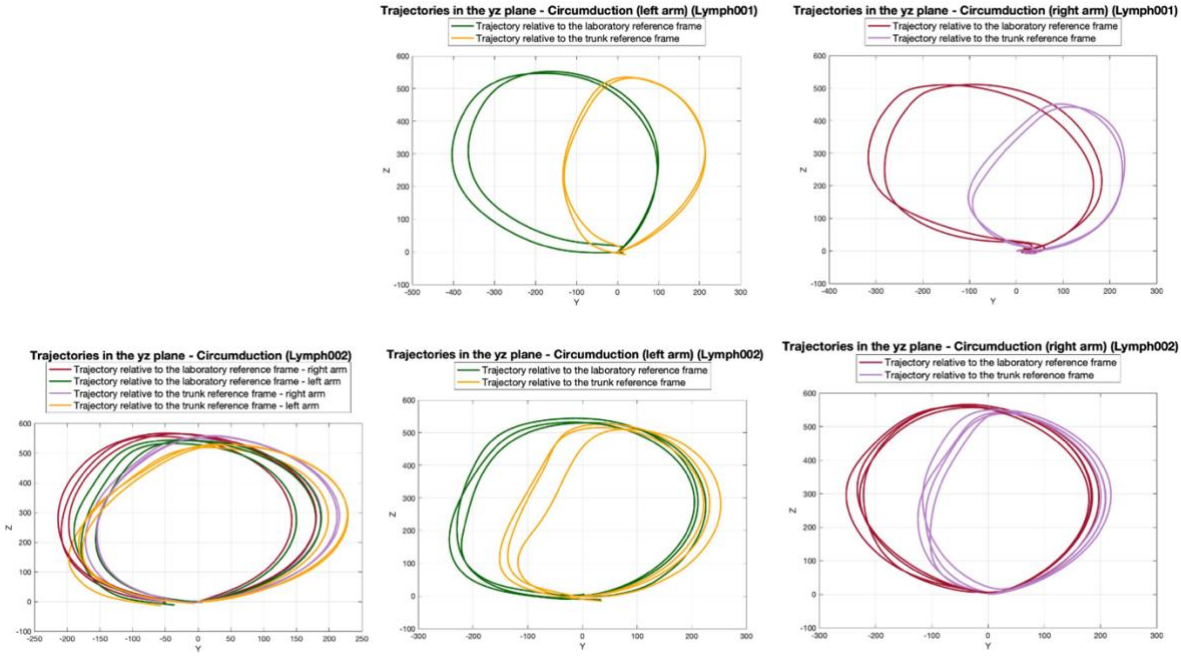

Figure 32. Trajectories of the circumduction tasks followed by both arms in the two patients. In the left column there are the trajectories of the circumduction task executed with both arms simultaneously, in the middle column there are the trajectories of the circumduction task executed with the unaffected arm, and in the right column there are the trajectories of the circumduction task executed with the arm affected by upper limb lymphedema.

3.2.3 *Comparison of the angles between trunk and pelvis*

To analyze the flexion-extension, abduction-adduction, and rotation angles between the trunk and pelvis, as well as between the pelvis and laboratory, the angular excursion from the initial movement point to reaching maximum amplitude has been considered.

Upon reviewing the results, it became evident that the angles between the pelvis and the laboratory showed minimal excursion (0-2°), making them inconsequential for the analysis objectives.

Instead, focusing on the angles between the trunk and pelvis, were evident the differences in angular excursion between functional tasks performed with one arm at a time in both control subjects and patients. To delve deeper into these differences, the variation in excursion between the arms has been computed.

Examining the flexion-extension angle variation (Figure 33), control subjects did not exhibit a clear pattern in trunk excursion, regardless of whether the movement was executed with the dominant or non-dominant upper limb. In contrast, patients showed increased angular excursion in the arm affected by upper limb lymphedema across all functional tasks, particularly in lateral and upward reaching tasks.

Regarding abduction-adduction angles (Figure 34), it was evident that for patient Lymphedema001, the difference in angular excursion between the arms was greater compared to controls and the other patient. Similarly, control subjects did not display a distinct pattern relative to trunk movement when performing tasks with either arm (only the difference in the frontal reaching task is statistically significant with p=0,014), while patient Lymphedema001 showed more trunk movement alignment with the affected arm during tasks. In the case of patient Lymphedema002, the variation values consistently fell within the range of those observed in control subjects. Trunk movement alignment with the affected arm was noticeable during frontal and lateral reaching tasks.

Lastly, observing the rotation angle (Figure 35), controls showed minimal differences in angular excursion between the arms in reaching tasks, whereas during circumduction tasks, most controls exhibited greater rotation when using the dominant arm. In control subjects the only significant difference, computed with the paired Wilcoxon test, in rotation angles excursion between the two arms emerges only in the upward reaching task (p=0,009). Patients, however, showed greater differences between arms, particularly patient Lymphedema001, who displayed more trunk rotation alignment with the affected arm in functional tasks, except during circumduction. Patient Lymphedema002 exhibited substantial variation in rotation angle excursion during frontal and lateral reaching tasks, aligning the trunk with the unaffected and affected arms, respectively.

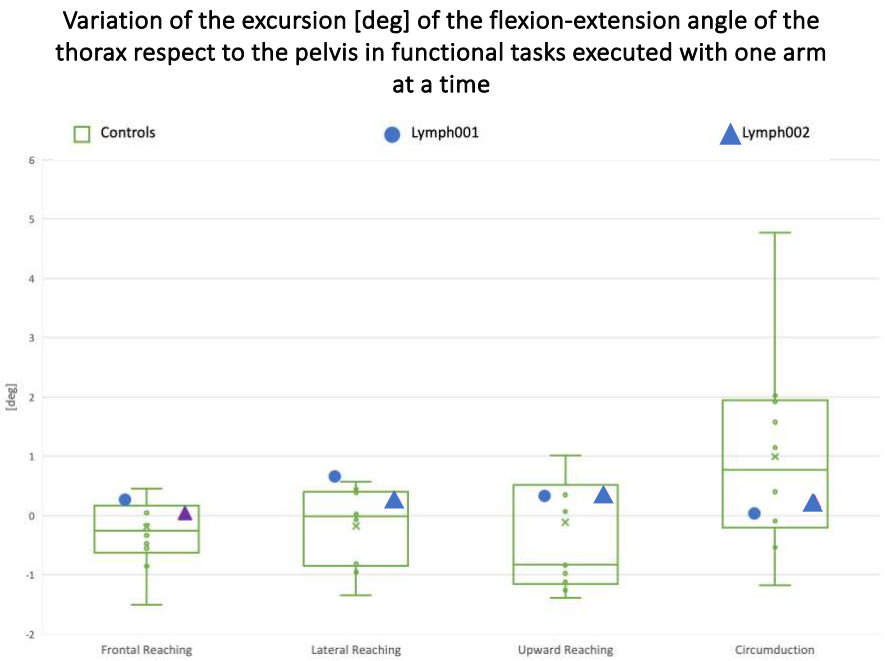

Figure 33. Variation in the excursion of the flexion-extension angle between thorax and pelvis by comparing angular excursion when the functional task is carried out with the non-dominant or affected upper limb to the excursion when the task is performed with the opposite arm. If the result is a positive value, there is more motion of the trunk during the non-dominant or affected upper limb movement. Instead, a negative variation means that the trunk compensatory action is greater when the movement is performed with the dominant or unaffected arm.

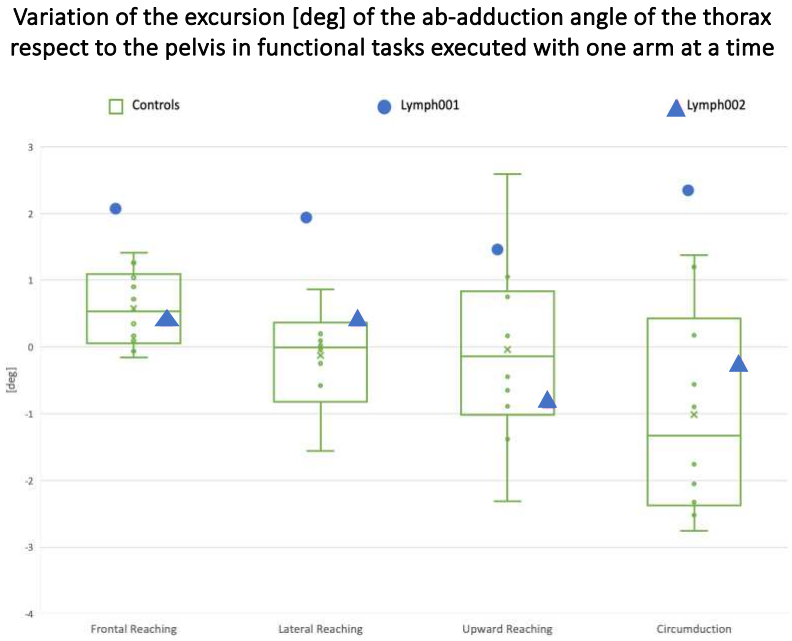

Figure 34. Variation in the excursion of the ab-adduction angle between thorax and pelvis by comparing angular excursion when the functional task is carried out with the non-dominant or affected upper limb to the excursion when the task is performed with the opposite arm. If the result is a positive value, there is more motion of the trunk during the non-dominant or affected upper limb movement. Instead, a negative

variation means that the trunk compensatory action is greater when the movement is performed with the dominant or unaffected arm.

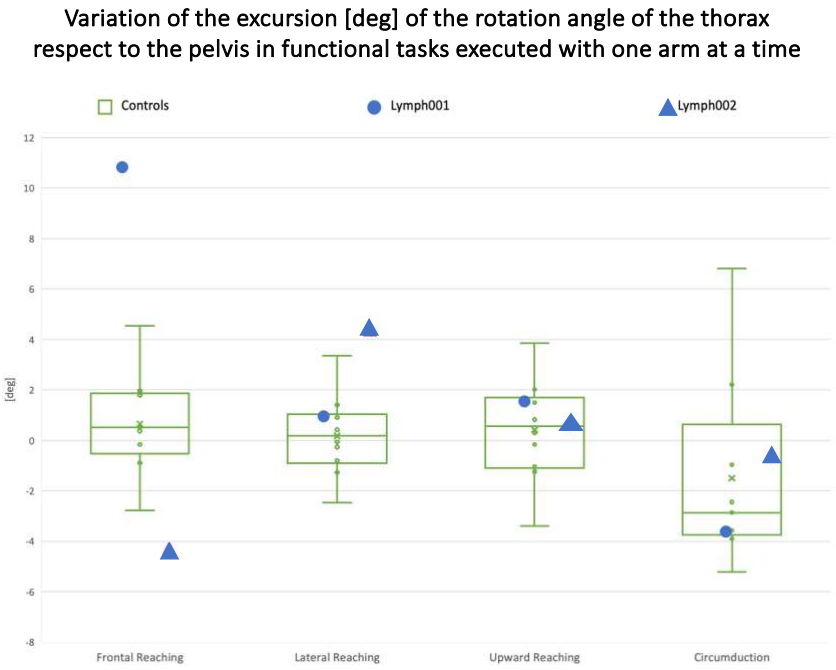

Figure 35. Variation in the excursion of the rotation angle between thorax and pelvis by comparing angular excursion when the functional task is carried out with the non-dominant or affected upper limb to the excursion when the task is performed with the opposite arm. If the result is a positive value, there is more motion of the trunk during the non-dominant or affected upper limb movement. Instead, a negative variation means that the trunk compensatory action is greater when the movement is performed with the dominant or unaffected arm.

DISCUSSION AND CONCLUSIONS

Through the investigation of upper limb kinematics during functional tasks, a nuanced understanding of how individuals, both healthy and those affected by lymphedema, execute these movements has been uncovered. The analysis delved into key metrics such as path length and velocity. Initially, when comparing path lengths between the dominant and non-dominant arms of healthy individuals, minimal discrepancies are discernible; slight variations are noted in reaching and circumduction tasks, where the path length with the dominant arm exceeds that with the non-dominant arm. Similarly, velocity values exhibit symmetry between the arms in most tasks, except for specific instances where the non-dominant arm demonstrates higher velocity due to its shorter path length. However, for both path length and velocity these differences are statistically significant in few cases. In contrast, individuals with upper limb lymphedema display more pronounced differences between affected and unaffected limbs concerning both path length and velocity. Across all functional tasks, the arm without lymphedema consistently covers a greater path length compared to the affected arm. Notably, even though the affected arm may exhibit a shorter path, the velocity values tend to be higher for the unaffected arm.

Furthermore, upon comparing the control group with the patient group, it becomes evident that individuals with lymphedema generally achieve lower path length values, especially notable in specific cases like subject Lymphedema001, which also reflects in their velocity values. This discrepancy highlights the impact of lymphedema on upper limb function, particularly in terms of movement range and speed. When assessing upper limb symmetry, notable variations in path length and velocity between the dominant and non-dominant arms or affected and unaffected limbs are observed, particularly in tasks performed with one arm at a time. For instance, asymmetry in path length and velocity is more pronounced in frontal and upward reaching for the patient Lymphedema001 and in lateral reaching for the patient Lymphedema002 compared to control subjects, indicating the influence of lymphedema on functional performance.

The investigation of the involvement of the trunk in upper limb functional tasks, particularly in comparing healthy subjects and patients, has been carried out through the analysis of various parameters, including shoulder displacement, trunk motion in different planes, and joint angles

between the trunk and pelvis, as well as between the pelvis and laboratory. Looking at these parameters, significant differences have been observed between the two groups. In examining shoulder displacement in the xy plane, indicative of trunk movement in the transverse plane, it was consistently noted that patients exhibited higher displacement values compared to control subjects across all functional tasks. This suggests a greater degree of trunk movement, encompassing both backward-forward and lateral movements, in patients during task execution. Furthermore, the asymmetry in trunk displacement between tasks executed with different arms was more pronounced within the patient group, particularly for patient Lymphedema001. Similarly, when analyzing trunk contribution in the sagittal plane during circumduction tasks, it was observed that patients displayed larger differences in trajectory amplitude between the laboratory and thorax reference frames, indicating increased trunk movement, especially when using the affected upper limb. This phenomenon highlights the significant role of the trunk in compensating for mobility limitations during upper limb motion in patients. Additionally, the analysis of joint angles between the trunk and pelvis revealed distinctions between control subjects and patients. Patients consistently exhibited increased angular excursion in the arm affected by upper limb lymphedema across various functional tasks, particularly in lateral and upward reaching tasks. This aligns with the observed greater trunk movement alignment with the affected arm during task execution in patients, further emphasizing the compensatory role of the trunk. Overall, the comparisons between healthy subjects and patients underscore the significant differences in trunk involvement during upper limb functional tasks. While control subjects generally displayed more symmetric and coordinated trunk movements, patients exhibited asymmetries and increased trunk involvement, particularly when using the affected upper limb. These findings contribute to a deeper understanding of how trunk and pelvis dynamics contribute to compensatory mechanisms in individuals with upper limb impairments.

In conclusion, the analysis of upper limb kinematics may serve as an evaluative index for monitoring the progression of treatment in the limb affected by lymphedema. By examining parameters such as path length, velocity, shoulder displacement, trunk motion, and joint angles, insights into the effectiveness of interventions may be gleaned. Specifically, deviations in these metrics from values obtained from control subjects or asymmetries between affected and unaffected limbs may indicate the need for adjustments in therapeutic approaches. For instance, consistent disparities in path length and velocity between the affected and unaffected arms may signify ongoing functional limitations despite treatment efforts. Moreover, the observed compensatory movements of the trunk underscore its pivotal role in adapting to upper limb impairments, implicating the need for interventions that address both limb-specific deficits and

associated trunk compensations. Overall, integrating kinematic analysis into clinical assessments could offer a comprehensive means of gauging treatment efficacy and tailoring therapeutic interventions to optimize functional outcomes for individuals with upper limb lymphedema.

REFERENCES

1. Maccarone MC, Venturini E, Menegatti E, Gianesini S, Masiero S. Water-based exercise for upper and lower limb lymphedema treatment. *J Vasc Surg Venous Lymphat Disord*. 2023;11(1):201-209. doi:10.1016/j.jvsv.2022.08.002
2. *THE DIAGNOSIS AND TREATMENT OF PERIPHERAL LYMPHEDEMA: 2020 CONSENSUS DOCUMENT OF THE INTERNATIONAL SOCIETY OF LYMPHOLOGY*.
3. Baran E, Yildiz Tİ, Gursen C, et al. The association of breast cancer-related lymphedema after unilateral mastectomy with shoulder girdle kinematics and upper extremity function. *J Biomech*. 2021;121. doi:10.1016/j.jbiomech.2021.110432
4. Li D, Wei H, Xiao L, Zhang R, Li Y. Stereo vision-based measurement of wave evolution around square column in laboratory. *Journal of Ocean Engineering and Science*. Published online 2023. doi:10.1016/j.joes.2023.10.002
5. Summan R, Pierce SG, Macleod CN, et al. Spatial calibration of large volume photogrammetry based metrology systems. *Measurement*. 2015;68:189-200. doi:10.1016/j.measurement.2015.02.054
6. Chiari L, Della Croce U, Leardini A, Cappozzo A. Human movement analysis using stereophotogrammetry. Part 2: Instrumental errors. *Gait Posture*. 2005;21(2):197-211. doi:10.1016/j.gaitpost.2004.04.004
7. Carse B, Meadows B, Bowers R, Rowe P. Affordable clinical gait analysis: An assessment of the marker tracking accuracy of a new low-cost optical 3D motion analysis system. *Physiotherapy (United Kingdom)*. 2013;99(4):347-351. doi:10.1016/j.physio.2013.03.001
8. Conconi M, Pompili A, Sancisi N, Parenti-Castelli V. Quantification of the errors associated with marker occlusion in stereophotogrammetric systems and implications on gait analysis. *J Biomech*. 2021;114. doi:10.1016/j.jbiomech.2020.110162
9. Matsuura D, Chounan Y, Omata M, Sugahara Y, Takeda Y. Gait analysis and regeneration by means of principal component analysis and its application to kinematic design of wearable walking assist device for hemiplegics. In: *Design and Operation of*

Human Locomotion Systems. Elsevier; 2020:33-49. doi:10.1016/B978-0-12-815659-9.00002-0

10. Plug-In Gait Reference Guide. *Plug-In Gait*. Accessed January 17, 2024. https://docs.vicon.com/display/Nexus212/Full+body+modeling+with+Plug-in+Gait
11. Woltring HJ. A Fortran package for generalized, cross-validatory spline smoothing and differentiation. *Advances in Engineering Software (1978)*. 1986;8(2):104-113. doi:10.1016/0141-1195(86)90098-7
12. Ton van den Bogert. *Practical Guide to Data Smoothing and Filtering*.; 1996.
13. Dario G. Liebermann, Joseph McIntyre, Mindy F. Levin, Patrice (Tamar) L. Weiss, Sigal Berman, Annual International Conference of the IEEE Engineering in Medicine and Biology Society 32 2010.08.31-09.04 Buenos Aires. Arm path fragmentation and spatiotemporal features of hand reaching in healthy subjects and stroke patients.
14. Šlajpah S, Čebašek E, Munih M, Mihelj M. Time-Based and Path-Based Analysis of Upper-Limb Movements during Activities of Daily Living. *Sensors*. 2023;23(3). doi:10.3390/s23031289
15. Mazzarella J, McNally M, Richie D, et al. 3d motion capture may detect spatiotemporal changes in pre-reaching upper extremity movements with and without a real-time constraint condition in infants with perinatal stroke and cerebral palsy: A longitudinal case series. *Sensors (Switzerland)*. 2020;20(24):1-17. doi:10.3390/s20247312
16. Mandon L, Boudarham J, Robertson J, Bensmail D, Roche N, Roby-Brami A. Faster reaching in chronic spastic stroke patients comes at the expense of arm-trunk coordination. *Neurorehabil Neural Repair*. 2016;30(3):209-220. doi:10.1177/1545968315591704
17. Monga P. *Three-Dimensional Analysis of Shoulder Movement Patterns in Shoulders with Anterior Instability: A Comparison of Kinematics with Normal Shoulders and the Influence of Stabilization Surgery*.; 2012.
18. Gates DH, Walters LS, Cowley J, Wilken JM, Resnik L. Range of motion requirements for upper-limb activities of daily living. *American Journal of Occupational Therapy*. 2016;70(1). doi:10.5014/ajot.2016.015487
19. Chen YW, Liao WW, Chen CL, Wu CY. Kinematic descriptions of upper limb function using simulated tasks in activities of daily living after stroke. *Hum Mov Sci*. 2021;79. doi:10.1016/j.humov.2021.102834

20. Peeters LHC, Kingma I, Faber GS, van Dieën JH, de Groot IJM. Trunk, head and pelvis interactions in healthy children when performing seated daily arm tasks. *Exp Brain Res*. 2018;236(7):2023-2036. doi:10.1007/s00221-018-5279-2

21. Grood ES, Suntay WJ. *A Joint Coordinate System for the Clinical Description of Three-Dimensional Motions: Application to the Knee 1*.; 1983. http://biomechanical.asmedigitalcollection.asme.org/